

Pro-UIGAN: Progressive Face Hallucination from Occluded Thumbnails

Yang Zhang, Xin Yu, Xiaobo Lu, Ping Liu

Abstract—In this paper, we study the task of hallucinating an authentic high-resolution (HR) face from an occluded thumbnail. We propose a multi-stage Progressive Upsampling and Inpainting Generative Adversarial Network, dubbed Pro-UIGAN, which exploits facial geometry priors to replenish and upsample ($8\times$) the occluded and tiny faces (16×16 pixels). Pro-UIGAN iteratively (1) estimates facial geometry priors for low-resolution (LR) faces and (2) acquires non-occluded HR face images under the guidance of the estimated priors. Our multi-stage hallucination network upsamples and inpaints occluded LR faces via a coarse-to-fine fashion, significantly reducing undesirable artifacts and blurriness. Specifically, we design a novel cross-modal transformer module for facial priors estimation, in which an input face and its landmark features are formulated as queries and keys, respectively. Such a design encourages joint feature learning across the input facial and landmark features, and deep feature correspondences will be discovered by attention. Thus, facial appearance features and facial geometry priors are learned in a mutual promotion manner. Extensive experiments show that our Pro-UIGAN attains visually pleasing completed HR faces, thus facilitating downstream tasks, *i.e.*, face alignment, face parsing, face recognition as well as expression classification.

Index Terms—Face inpainting, super-resolution, face hallucination, generative adversarial network.

I. INTRODUCTION

With the increasing demand for social security, non-intrusive identity verification has become indispensable in daily life. As face is one of the most frequently utilized biometric cues, it is highly desirable to obtain face images in high quality in order to provide essential information for identity verification. However, in real scenarios, such as in surveillance systems, the captured faces usually not only are in low resolutions but also undergo occlusions caused by body parts or accessories, such as eye-glasses, scarves, etc. Since the information available in those low-resolution (LR) face images with occlusions is quite limited, it is difficult to extract useful features to support downstream applications, such as

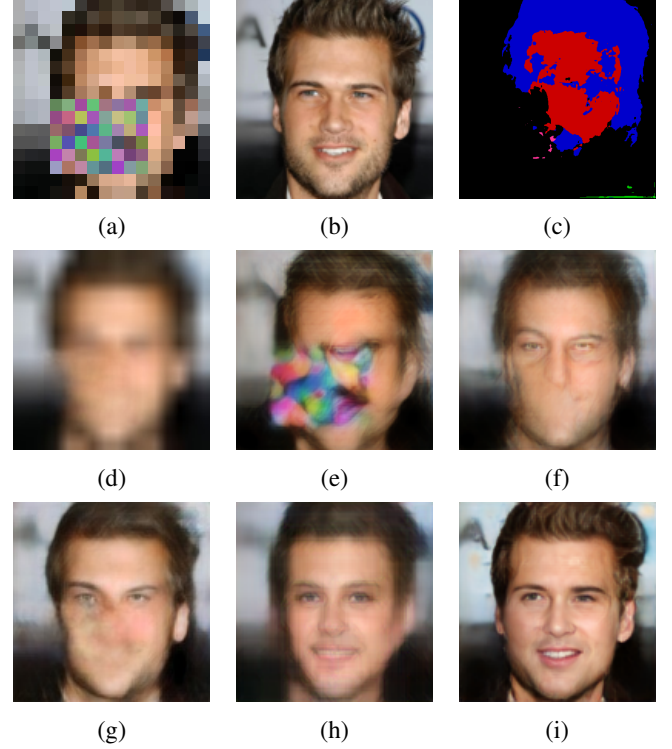


Fig. 1: Face inpainting and upsampling results on an occluded LR face. (a) The 16×16 occluded LR face image. (b) The original 128×128 non-occluded HR face image. (c) Face parsing result of (a), which is obtained by applying bicubic interpolation followed by the work [1]. (d) Face inpainting result of (a), which is obtained by applying bicubic interpolation followed by the work [2]. (e) Face SR result of (a) by applying [3]. (f) Result obtained by applying [2] followed by [3]. (g) Result obtained by applying [3] followed by [2]. (h) Result of FCSR-GAN [4]. (i) Result of our Pro-UIGAN.

face verification and facial attribute classification. Therefore, it becomes necessary to design advanced methods to hallucinate LR images and uncover the information from occlusions.

One straightforward solution to hallucinating LR face images with occlusions is directly utilizing existing face SR methods [3], [5]–[9] and face inpainting solutions [2], [10] to process the LR images with occlusions, which, however, has been experimentally proved sub-optimal. On the one hand, off-the-shelf face inpainting methods usually require a high-resolution (HR) face image as their inputs to analyze the context in facial regions. When the input images are in low

Y. Zhang is with the Key Laboratory of Intelligent Perception and Systems for High-Dimensional Information, Ministry of Education, School of Computer Science and Engineering, Nanjing University of Science and Technology, Nanjing 210094, China, e-mail: zhangyang201703@126.com.

X. Yu is with the Australian Institute of Artificial Intelligence, University of Technology Sydney, Ultimo, NSW 2007, Australia, e-mail: xin.yu@uts.edu.au.

X. B. Lu is with the School of Automation, Southeast University, Nanjing 210096, China; Key Laboratory of Measurement and Control of Complex Systems of Engineering, Ministry of Education, Nanjing 210096, China, e-mail: xblu2013@126.com.

P. Liu (corresponding author) is with the Institute of High Performance Computing, Research Agency for Science, Technology and Research (A*STAR), Singapore 138634, e-mail: pino.pingliu@gmail.com.

resolutions, for example, 16×16 pixels, it becomes impractical to accurately segment the facial areas (see Fig. 1(c)), let alone conducting further analysis and modeling on each facial component. Hence, inpainting leads to overly-blurred facial details (see Fig. 1(d)). Those errors might be exaggerated in the following face SR process (see Fig. 1(f)). On the other hand, most of existing face SR solutions only consider non-occluded face images as their inputs. These methods may suffer from ghosting artifacts in the results when LR inputs with occlusions are given (see Fig. 1(e)). Moreover, when we apply face inpainting methods on those hallucinated images, the final results will exhibit severe distortions (see Fig. 1(g)). Based on our observations, we believe that treating face SR and face inpainting as two independent tasks is not an ideal solution.

Very recently, [4] proposes a deep generative adversarial network (FCSR-GAN) to jointly super-resolve and inpaint occluded face images in low resolutions. Compared to the solutions which directly combine face inpainting and SR methods, FCSR-GAN is able to alleviate artifacts to some extent. However, FCSR-GAN may output blurry results when the inputs have very low resolutions and extreme poses. As shown in Fig. 1(h), over-smoothed facial details and severe distortions appear in the hallucinated face.

In this paper, we propose to hallucinate occluded LR inputs¹ while achieving non-occluded HR faces² in a unified framework. In this manner, these two tasks (*i.e.*, face SR and face inpainting) are addressed simultaneously and mutually facilitate each other. Moreover, we design a progressive joint face SR and face inpainting framework, dubbed Pro-UIGAN. Pro-UIGAN runs in a multi-stage manner where each stage refines the face images hallucinated at the previous stage. By iteratively refining the details of hallucinated images, we can achieve high-quality results for large upsampling factors. Not only that, equipped with a delicate designed cross-modal attention mechanism, we exploit facial geometry priors (*i.e.*, facial landmark heatmaps) as the semantic guidance during our progressive hallucination process to reconstruct more realistic facial details.

Our Pro-UIGAN consists of a Pro-UI-net and two discriminators, *i.e.*, a local discriminator (namely Local-D) and a global discriminator (namely Global-D). The Pro-UI-net stacks a few successive Upsampling and Inpainting Blocks (UI-blocks) and generates a non-occluded HR face image by performing multiple inpainting and upsampling of an occluded LR face. By doing so, we can inpaint and super-resolve the LR input in a coarse-to-fine manner. In particular, in each stage, our UI-block comprises a Cross-modal Transformer Module (CM-TM) and a Transformative Upsampling Net (TUN). It estimates the most distinguishable facial landmarks in an input face and constructs facial geometry priors to guide hallucination. Our designed CM-TM employs the input face and its landmark features as queries and keys to calculate their cross-attention matrix for deep feature correspondences construction. Then, it generates facial geometry priors and facial appearance

features in a mutual promotion manner. In our multi-stage hallucination process, the first UI-block generates a coarse hallucinated face from the occluded LR input, which acts as a preliminary result for following UI-blocks. Then, the following UI-blocks refine the face images hallucinated at the previous stage and generate hallucination results with finer details. Fig. 1(i) illustrates that our hallucinated non-occluded HR face is more photo-realistic than the results of the state-of-the-art.

Overall, our contributions are fourfold:

- We present a novel framework, namely Progressive Upsampling and Inpainting Generative Adversarial Network (Pro-UIGAN), to jointly achieve face inpainting and face SR in a unified framework.
- We design a multi-stage hallucination and inpainting interwoven strategy. Specifically, we upsample and inpaint occluded LR faces via a coarse-to-fine fashion, thereby reducing undesirable artifacts and noises compared to a direct combination of face hallucination and inpainting methods.
- We propose a Cross-Modal Transformer Module (CM-TM) to collaboratively learn facial geometry priors and facial appearance features. Our CM-TM provides effective clues for feature alignment and enhancement, and thus promotes more accurate face hallucination results.
- Extensive experiments manifest that Pro-UIGAN authentically replenishes ($8\times$ upsampling) occluded and low-resolution face images (*i.e.*, 16×16 pixels). Moreover, our Pro-UIGAN provides superior hallucinated face images for downstream tasks, *i.e.*, face alignment, face parsing, face recognition as well as expression classification, in comparison to the SotA.

II. RELATED WORK

A. Face Super-resolution

Face Super-resolution (SR) aims at enhancing the resolution of LR face images to generate corresponding HR face images. The previous works can be generally grouped into three categories: holistic-based [11]–[13], part-based [14]–[20], as well as deep learning based solutions [3], [6], [21]–[28].

Holistic-based methods employ global face models to up-sample LR faces. Wang *et al.* [11] establish a linear mapping between LR and HR images to achieve face SR based on an Eigen-transformation of LR faces. Liu *et al.* [12] incorporate a bilateral filtering to mitigate the ghosting artifacts, improving the quality of generated HR faces. Kolouri and Rohde [13] introduce optimal transport and subspace learning to morph HR faces from aligned LR ones. However, they require LR inputs to be precisely aligned, and reference HR faces are under canonical poses and natural expressions.

To handle large poses and complex expressions, part-based methods have been proposed to super-resolve local facial regions rather than enforcing global constraints. The works [14]–[17] incorporate facial patches extracted from HR datasets to enhance input LR facial regions. Marshall *et al.* [19] employ the SIFT Flow algorithm to warp exemplar faces and compute the hallucinated HR image through MAP estimation.

¹occluded LR faces: low-resolution faces with occlusions.

²non-occluded HR faces: high-resolution faces without occlusions.

Yang *et al.* [20] use facial landmarks to retrieve adequate high-resolution facial component exemplars for further face super-resolution. Those works [19], [20] need to precisely localize facial components for face super-resolution, which is challenging, especially in LR cases.

Benefiting from the strong feature extraction ability of deep neural networks, deep learning-based solutions achieve promising performance compared to traditional techniques. Yu *et al.* [21] design a GAN-based model to upsample LR faces. Huang *et al.* [22] introduce wavelet coefficients into CNNs to super-resolve LR faces with multiple upscaling factors. Cao *et al.* [6] put forward an attention-aware mechanism and a local enhancement network to progressively enhance local facial regions during hallucination. Xu *et al.* [24] exploit a multi-class adversarial loss to promote joint face SR and deblurring. Dahl *et al.* [25] propose to super-resolve pre-aligned LR inputs via designing an autoregressive Pixel-RNN [26]. Yu *et al.* [3] incorporate facial component information from the intermediate upsampled features into an upsampling stream to achieve superior face hallucination results. Yu *et al.* [27] present a multiscale transformative discriminative neural network to super-resolve unaligned and very small faces of variable resolutions. Zhang *et al.* [28] present a two-branch upsampling framework to normalize and super-resolve non-uniform illumination and low-resolution inputs. Menon *et al.* [9] present a Photo Upsampling via Latent Space Exploration (PULSE) algorithm to generate high-quality frontal face images at large resolutions. Since those works [3], [6], [9], [21]–[28] aim to super-resolve LR faces without occlusions, they might obtain inferior results when occluded LR inputs are given, as seen in Fig. 1(e).

B. Image Inpainting

Image inpainting is to generate missing regions in corrupted images. The inpainted images should be not only visually realistic but also consistent in content. Image inpainting techniques can be divided into three categories. The first category employs the diffusion equation to iteratively propagate low-level features from the content area to the missing region along the boundaries [30], [31]. The methods belonging to the second category are patch-based methods, which search similar patches from the same image or exemplar image databases to fill in the missing contents [32]–[35]. The third category is learning-based methods, which employ encoder-decoder networks to extract image features and generate missing content according to the extracted features [36], [37]. However, these methods generally focus on inpainting natural images rather than class-specific images, such as faces.

Face inpainting is even more challenging because the face topological structure and the face identity should be retained during the inpainting process and humans are very sensitive to distorted facial structure. In general, researchers usually introduce facial prior information to inpainting. S. Zhang *et al.* [38] aim to recover face images from structural obstructions such as streaks. However, their method is more effective when only a small area is missing. Li *et al.* [2] propose a face inpainting GAN which introduces facial geometry as semantic regularization to maintain face topological structure.

Meanwhile, they use both global and local discriminators to ensure the quality of completed face images. However, their algorithm is sensitive to pose and expression variations and may fail when the occluded faces are in low resolutions. [10] designs a geometry-aware face inpainting model which exploits facial geometry information as guidance for inpainting. Liu *et al.* [39] integrate perceptual subnetwork to capture semantic-level facial features, thus improving synthesized content details. While these methods [10], [39] focus on the correctness of the structural information, they neglect the quality of the texture on key areas in the image (*e.g.*, key facial components). Zhou *et al.* [40] propose to learn the correlations between facial textures at multiple scales and take the location of the facial components as prior knowledge during the face inpainting process. Although [40] can produce high-fidelity face images with fine-grained facial components, it still suffers from severe performance degradation when inputs are in low resolutions.

III. PROPOSED METHOD: PRO-UIGAN

In this section, we propose a Progressive Upsampling and Inpainting Generative Adversarial Network (Pro-UIGAN) for joint face inpainting and SR. Our Pro-UIGAN comprises a Pro-UIInet and two discriminators, *i.e.*, Local-D and Global-D. The Pro-UIInet estimates facial geometry priors, *i.e.*, facial landmark heatmaps, and uses them as the semantic guidance to obtain non-occluded HR faces progressively. Meanwhile, the Local-D and Global-D enforce the hallucinated faces to be more photo-realistic.

A. Multi-stage Progressive Hallucination Strategy

Inspired by Bengio *et al.* [41], we define a reasonable multi-stage progressive hallucination strategy. The first stage produces a coarse hallucinated face from an occluded LR input, which acts as a preliminary result for its following stage to refine. Then, the following stage achieves refinement of the face image hallucinated at the previous stage and generates a finer hallucinated one, which provides more delicate prior knowledge for the next stage. By repeating procedures mentioned previously, we can super-resolve and inpaint the occluded LR face in a coarse-to-fine manner. It is empirically demonstrated that our proposed progressive learning manner and the designed network can reduce blurriness and artifacts in the hallucinated face image significantly, as shown in Fig. 4(l).

B. Pro-UIInet

Based on our multi-stage progressive hallucination strategy, our Pro-UIInet stacks a series of Upsampling and Inpainting Blocks (UI-blocks) and reconstructs non-occluded HR face images progressively (see Fig. 2).

First, an occluded LR face and its facial landmark features estimated by [29] are sent into the first UI-block. Our UI-block comprises a Cross-Modal Transformer Module (CM-TM) and a Transformative Upsampling Net (TUN). The CM-TM employs the input face and its landmark features as queries and keys, and collaboratively learns facial geometry priors and

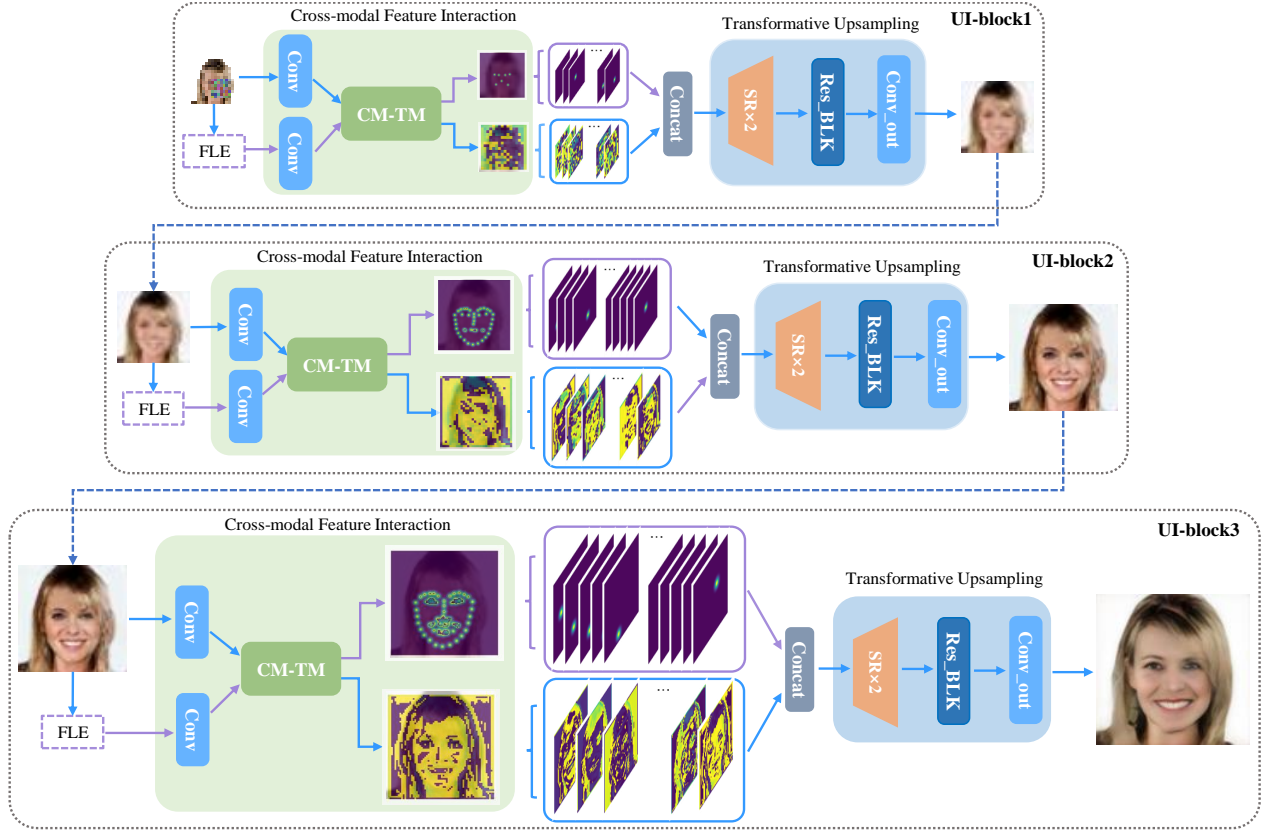


Fig. 2: The architecture of our Pro-UInet. Here, FLE represents a facial landmark estimation model [29]. CM-TM represents the cross-modal transformer module.

facial appearance features. Then, the learned facial geometry priors and facial appearance features are concentrated and sent into the TUN for feature alignment, aggregation, and $2\times$ upscaling. Our TUN employs the residual block [42] to enhance high-frequency facial details while improving the network capacity. As a result, the first UI-block generates a coarse completed and upsampled face (see Fig. 4(c)). Subsequently, the latter UI-blocks further inpaint and upsample the coarse hallucinated face, generating finer hallucinated ones (see Figs. 4(d) and (l)). Specifically, as the stage number increases, the latest input image generated by the UI-block in the past stage, becomes more accurate in structures and provides more detailed prior knowledge, both of which benefit to learning processes in the current and following stages.

C. Cross-modal Transformer Module (CM-TM)

We argue that facial geometry priors (*i.e.*, facial landmark heatmaps) and facial appearance features are different but complementary. Thus, we design the CM-TM to learn facial geometry priors and facial appearance features in a mutual promotion manner.

As shown in Fig. 3, the facial landmark features F_L and the input facial features F_C are formulated as queries (Q) and keys (K) to calculate their cross-attention matrix. Then, the cross-attention matrix is adopted to augment the attended features from one stream to another. Such a design encourages joint feature learning across the input facial and landmark features,

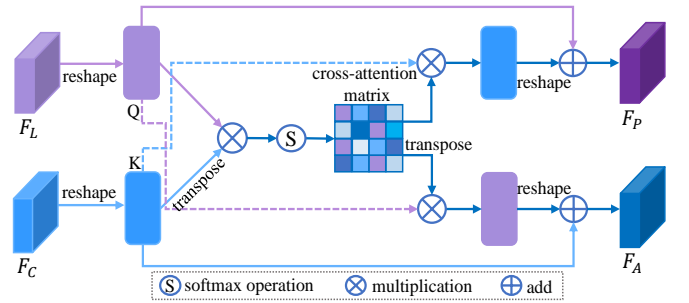


Fig. 3: The diagram of CM-TM. F_L , F_C , F_P and F_A represent facial landmark features, input facial features, facial geometry priors and facial appearance features, respectively.

and their deep feature correspondences will be discovered by attention. As a result, we can learn the facial geometry priors (F_P) and facial appearance features (F_A).

To illustrate the effect of our CM-TM, we conduct some comparisons. Fig. 4(e) shows that the Pro-UIGAN variant without CM-TM produces inferior results. Therefore, our CM-TM provides effective facial geometry priors as clues for feature alignment and enhancement, and thus promotes more accurate face hallucination results (see Fig. 4(l)).

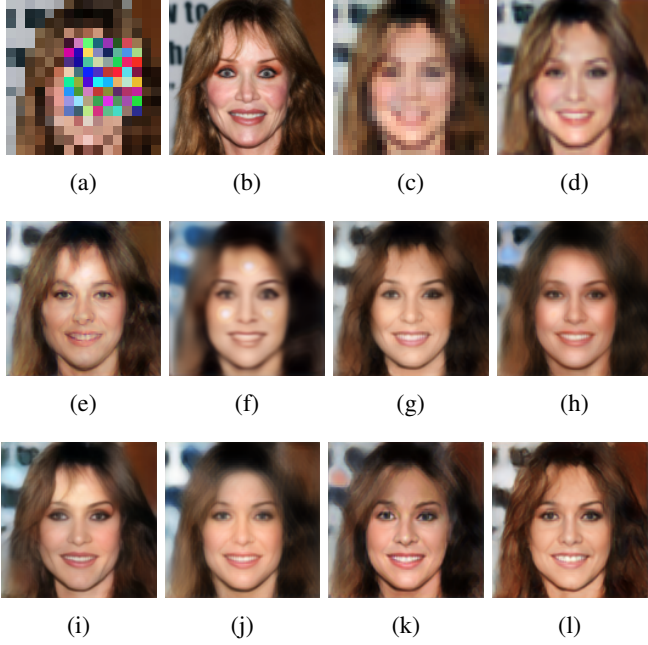


Fig. 4: Impacts of different components and losses on model performance. (a) Occluded LR images (16×16 pixels). (b) Ground-truth HR images (128×128 pixels). (c) Results of UI-block1. (d) Results of UI-block2. (e) Results of Pro-UIGAN without adopting CM-TMs. Note that the facial geometry is ambiguous. (f) Results of Pro-UIGAN trained by L_{mse} and L_h . (g) Results of Pro-UIGAN trained by L_{mse} , L_{id} and L_h . (h) Results of Pro-UIGAN without using the estimated facial geometry priors. Here, we just employ the facial appearance features as the input of TUNs. (i) Results of Pro-UIGAN using ground-truth facial geometry priors. (j) Results of Pro-UInet (Pro-UIGAN trained without employing L_{adv}^l and L_{adv}^g). (k) Results of Pro-UInet and Local-D. (l) Results of Pro-UIGAN.

D. Local-Global Discriminators

Our Pro-UInet upsamples occluded LR faces through a coarse-to-fine fashion and generates non-occluded HR face images. We employ two discriminators, *i.e.*, Global-D and Local-D, to force the generated HR faces to lie on the same manifold as real HR faces do. The Local-D encourages the newly generated missing parts to be semantically valid, while the Global-D focuses on the whole faces for more photo-realistic global views.

To dissect the impacts of Global-D and Local-D, we provide the results of different Pro-UIGAN variants (see Figs. 4(j), (k), and (l)). As shown in Fig. 4(k), the Pro-UInet with Local-D generates visually pleasing details of missing components. However, the global structure of the face is still blurry. This is because the Local-D can hardly generate a direct impact outside the missing regions during the back propagation. In contrast, as shown in Fig. 4(l), our Pro-UIGAN captures global profiles of faces and local facial characteristics.

E. Objective Functions

We incorporate six independent losses for training our Pro-UIGAN, including an intensity similarity loss (L_{mse}), an

identity similarity loss (L_{id}), a mirror symmetry loss (L_{sys}), a geometry similarity loss (L_h), a style loss (L_{style}) and a local-global discriminative loss (L_{adv}^l and L_{adv}^g).

1) *Intensity similarity loss*: We constrain the hallucinated face to be close to the ground-truth in terms of image intensities. Therefore, we employ an intensity similarity loss L_{mse} , expressed as:

$$L_{mse} = \mathbb{E}_{(\hat{h}_i, h_i) \sim p(\hat{h}, h)} \|\hat{h}_i - h_i\|_F^2, \quad (1)$$

where $p(\hat{h}, h)$ represents the joint distribution of the hallucinated face \hat{h}_i and the corresponding ground-truth h_i .

2) *Identity similarity loss*: As the intensity similarity loss L_{mse} leads to over-smoothed results [43] (see Fig. 4(f)), we introduce an identity similarity loss [44] to improve our hallucinated faces. The identity similarity loss L_{id} measures the Euclidean distance between the high-level features of a hallucinated face and its ground-truth, written as:

$$L_{id} = \mathbb{E}_{(\hat{h}_i, h_i) \sim p(\hat{h}, h)} \|\Phi(\hat{h}_i) - \Phi(h_i)\|_F^2, \quad (2)$$

where $\Phi(\cdot)$ represents the extracted feature maps of a layer in VGG-19 [45]. We use the layer ReLU32, which gives good empirical results in our experiments. As seen in Fig. 4(g), exploiting L_{id} results in better hallucinated results with more photo-realistic facial details.

3) *Mirror symmetry loss*: In order to guarantee the content integrity of hallucinated faces, we use a mirror symmetry loss [46]. The mirror symmetry loss L_{sys} for an upsampled face \hat{h}_i is defined as:

$$L_{sym} = \mathbb{E}_{(\hat{h}_i) \sim p(\hat{h})} \|\vec{\hat{h}}_i - \hat{h}_i\|_F^2, \quad (3)$$

where $\vec{\hat{h}}_i$ is the horizontally flipped copy of \hat{h}_i .

4) *Geometry similarity loss*: Aiming at facilitating face alignment as well as constraining the topological structure consistency between the generated HR image and the ground-truth one, a geometry similarity loss L_h [47] is employed in training our CM-TMs, expressed as:

$$L_h = \mathbb{E}_{(l_i, h_i) \sim p(l, h)} \frac{1}{L} \sum_{l=1}^L \|H^k(f_i) - H^k(h_i)\|_2^2, \quad (4)$$

where $H^k(f_i)$ represents the estimated k -th facial landmark heatmap by our CM-TM. $H^k(h_i)$ denotes the corresponding facial landmark heatmap generated by FAN [29] on the ground-truth image h_i .

5) *Style loss*: Inspired by [48], we introduce a style loss L_{style} to enforce the style of the completed area as similar as possible to the ground-truth image. The style loss L_{style} is defined as:

$$L_{style} = \sum_{n=0}^{N-1} \left\| K_n \left(\phi_n(\hat{h}_i)^T \phi_n(\hat{h}_i) - \phi_n(h_i)^T \phi_n(h_i) \right) \right\|_1, \quad (5)$$

where $\phi_n(\cdot)$ represents the extracted feature maps of the n -th layer in VGG-16 [45], and we use the pool1, pool2 and pool3 layers. $K_n = 1 / (C_n \cdot H_n \cdot W_n)$ is a normalization factor for the n -th VGG-16 layer. C_n , H_n , and W_n are the channel number, height, and width of the feature maps, respectively.

6) *Local-Global discriminative loss*: In order to generate visually appealing results, we incorporate class-specific discriminative information into our Pro-UINet by employing local-global discriminators, *i.e.*, Local-D and Global-D. Our goal is to fool the local-global discriminators and make them fail to classify hallucinated images and real ones.

The objective function L_D^l for the Local-D is defined as follows:

$$L_D^l = -\mathbb{E}_{(\hat{m}_i, m_i) \sim p(\hat{m}, m)} \left[\log D_u^l(m_i) + \log(1 - D_u^l(\hat{m}_i)) \right], \quad (6)$$

where $p(\hat{m}, m)$ represents the joint distribution of reconstructed occluded areas \hat{m}_i and corresponding ground-truths m_i . D^l and u represent the Local-D and its parameters. To make the Local-D distinguish hallucinated occluded areas from real ones, we minimize the loss L_D^l and update its parameters u .

The objective function L_D^g for the Global-D is defined as follows:

$$L_D^g = -\mathbb{E}_{(\hat{h}_i, h_i) \sim p(\hat{h}, h)} \left[\log D_v^g(h_i) + \log(1 - D_v^g(\hat{h}_i)) \right], \quad (7)$$

where D^g and v represent the Global-D and its parameters. To enable the Global-D to distinguish hallucinated faces from real ones, we minimize the loss L_D^g and update its parameters v .

For the generator in our Pro-UINet, it aims to fool the local-global discriminators by producing realistic non-occluded HR faces.

Thus, the local discriminative loss L_{adv}^l is written as:

$$L_{adv}^l = -\mathbb{E}_{\hat{m}_i \sim p(\hat{m})} \log(D_u^l(\hat{m}_i)). \quad (8)$$

Meanwhile, the global discriminative loss L_{adv}^g is represented as:

$$L_{adv}^g = -\mathbb{E}_{\hat{h}_i \sim p(\hat{h})} \log(D_v^g(\hat{h}_i)). \quad (9)$$

In the network learning process, we minimize L_{adv}^l and L_{adv}^g .

F. Training Details

Although UI-block1, UI-block2, and UI-block3 tackle the same hallucination subtask, their different inputs with diverse details attach their learning process with varying levels of difficulty. Therefore, we adopt different loss terms for training different UI-blocks.

The objective function for the UI-block1, L_{net1} , is expressed as:

$$L_{net1} = L_{sys}^a + L_{mse}^a + \alpha L_{id}^a + \beta L_h^a + \gamma^a L_{style}^a. \quad (10)$$

The objective function for the UI-block2, L_{net2} , is expressed as:

$$L_{net2} = L_{mse}^b + \alpha L_{id}^b + \beta L_h^b + \gamma^b L_{style}^b. \quad (11)$$

The objective function for the UI-block3, L_{net3} , is expressed as:

$$L_{net3} = L_{mse}^c + \alpha L_{id}^c + \beta L_h^c + \gamma^c L_{style}^c + \psi(L_{adv}^l + L_{adv}^g). \quad (12)$$

Consequently, the total objective function of our Pro-UINet, L_G is written as:

$$L_G = L_{net1} + L_{net2} + L_{net3}. \quad (13)$$

Since we aim to force hallucinated HR faces to be similar to real ones, we set lower weights on L_{id} , L_h , L_{adv}^l and L_{adv}^g . Thus, α, β and ψ in Eqs. (10)–(12) are set to 0.01. Meanwhile, γ^a, γ^b and γ^c are set to 10, 10 and 1, respectively.

The training procedure of our Pro-UIGAN model includes three steps: (i) Pre-training the UI-block1 with loss L_{net1} (Eq. (10)) so as to initialize model parameter. (ii) Pre-training the UI-block2 with loss L_{net2} (Eq. (11)). In this stage, the UI-block1 has been initialized. (iii) Training the whole Pro-UIGAN model: Pro-UINet is trained by L_G (Eq. (13)), and L_D^l (Eq. (6)) and L_D^g (Eq. (7)) are used to optimize Local-D and Global-D. In step (iii), since our UI-block1 and UI-block2 have been initialized, the learning rates for training UI-block3, UI-block2, and UI-block1 are set to 10^{-3} , 10^{-4} , and 10^{-4} , respectively.

IV. EXPERIMENTS

A. Experimental Setup

1) *Databases*: Our Pro-UIGAN is trained and tested on popular face databases, *i.e.*, the CelebA-HQ database [49], the Multi-PIE database [50], and the Helen database [51].

Multi-PIE [50] provides 750K+ images of 337 individuals under different conditions. We select 12,912 images of all the individuals spanning across various poses (0° , $\pm 15^\circ$, $\pm 30^\circ$, $\pm 45^\circ$, $\pm 60^\circ$, $\pm 75^\circ$, $\pm 90^\circ$) as well as expressions (“squint”, “disgust”, “neutral”, “smile”, “surprise”, and “scream”). Our training set contains 12,000 images belonging to the former 250 individuals, and the testing set includes 912 images belonging to the remaining 87 individuals.

CelebA-HQ [52] consists of 30,000 high-resolution face images under various poses, expressions and backgrounds. Each face image has a manually annotated, binary segmentation mask as well as 19 labeled facial attributes, *e.g.*, eyes, mouth, hat, neck, skin, etc. We employ the standard split for CelebA-HQ in our experiments, where 28,432 images for training and 1,568 for testing.

Helen [51] is composed of 2,330 in-the-wild face images with labeled facial components, *e.g.*, eyebrows, lips, nose, skin, hairs, etc. We use the former 2,280 images to construct the training set, and the remaining 50 images form the testing set. Specifically, we conduct data augmentation for the training set. We rotate the face images by $\pm 90^\circ$, $\pm 180^\circ$, $\pm 270^\circ$ and then flip them horizontally. As a result, we augment seven additional images for each original one.

2) *Implementation details*: First, faces in all the databases are detected, cropped, and resized to 128×128 pixels and thus form our ground-truths. Then, we use the masks with different sizes, ranging from 16×16 to 64×64 pixels, and covering at least one critical facial component to construct the occluded HR faces. Note that the position of the mask is randomly selected. Afterward, we generate the occluded LR faces (16×16 pixels) by transforming and downsampling the occluded HR ones. As a result, we construct occluded LR/non-occluded HR face pairs for each database. Our large-scale occluded LR/non-occluded HR face pair dataset and the code will be available on <https://github.com/SEU-yang>.

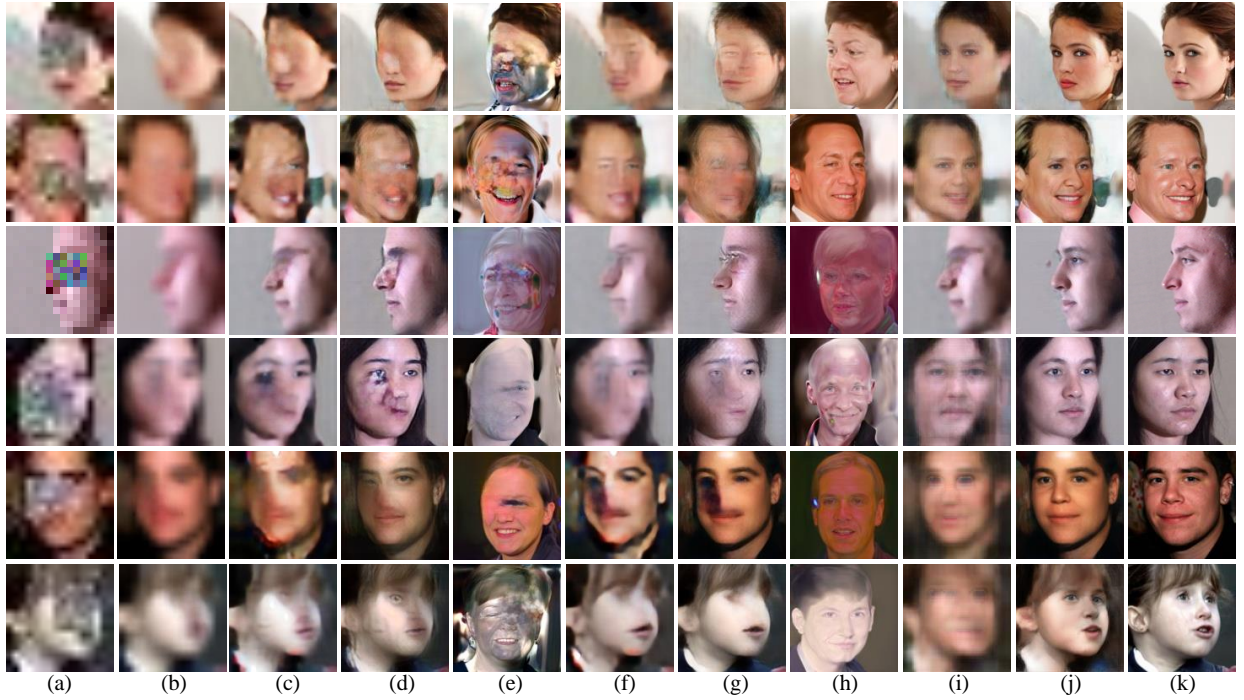


Fig. 5: Qualitative comparisons of competing methods on the **CelebA-HQ**, **Multi-PIE**, and **Helen** databases. Columns: (a) Occluded LR faces (16×16 pixels). (b) Bicubic + [2] (c) [7] + [2]. (d) [3] + [2]. (e) [9] + [2]. (f) [2] + [7]. (g) [2] + [3]. (h) [2] + [9]. (i) [4]. (j) Ours. (k) Ground-truths. The first two lines: testing samples from **CelebA-HQ**. The middle two lines: testing samples from **Multi-PIE**. The last two lines: testing samples from **Helen**.

TABLE I: Quantitative comparisons of competing methods on the **CelebA-HQ**, **Multi-PIE**, and **Helen** databases.

SR Method	CelebA-HQ		Multi-PIE		Helen		CelebA-HQ		Multi-PIE		Helen	
	SR+PA [2]						PA [2]+SR					
	PSNR	SSIM	PSNR	SSIM	PSNR	SSIM	PSNR	SSIM	PSNR	SSIM	PSNR	SSIM
Bicubic	14.038	0.411	12.761	0.370	13.665	0.389	15.322	0.457	14.215	0.416	13.763	0.392
FSRnet [7]	15.011	0.451	13.538	0.403	14.086	0.423	16.445	0.482	15.386	0.459	14.342	0.420
FHC [3]	16.950	0.503	16.448	0.482	16.003	0.476	19.224	0.609	18.198	0.573	17.715	0.546
PULSE [9]	13.106	0.353	8.451	0.182	10.516	0.273	15.270	0.456	9.237	0.206	11.128	0.294
FCSR-GAN [4]	23.010	0.698	21.327	0.649	20.745	0.627	23.010	0.698	21.327	0.649	20.745	0.627
Pro-UIGAN	25.470	0.763	23.188	0.704	22.038	0.659	25.470	0.763	23.188	0.704	22.038	0.659

3) *Competing methods*: We conduct comparative experiments in the following three manners:

- SR+PA: face SR methods (FSRnet [7], FHC [3], or PULSE [9]) followed by face inpainting techniques (GFC [2]);
- PA+SR: face inpainting techniques (GFC [2]) followed by face SR methods (FSRnet [7], FHC [3], or PULSE [9]) (bicubic interpolation is used to resize images);
- Joint SR+PA: FCSR-GAN [4] and our Pro-UIGAN.

In the first manner (SR+PA), we upsample the occluded LR faces first and then inpaint the upscaled results. In the second manner (PA+SR), we first inpaint occluded LR faces by widely-used face inpainting techniques and then upsample the completed faces by SotA face SR methods. In the third manner (Joint SR+PA), both FCSR-GAN [4] and Pro-UIGAN handle face SR and face inpainting in a unified framework. Here, we retrain these compared methods on our training datasets for fair comparisons.

B. Qualitative Evaluation

Fig. 5 illustrates the qualitative results of the compared methods.

As visible in Fig. 5(b), different combinations of bicubic interpolation and face inpainting methods [2] fail to reconstruct authentic facial details. Because bicubic only interpolates new pixels from neighboring ones, it can not produce new contents and upsampled HR images lack details. Consequently, the face inpainting method fails to segment facial areas and generates erroneous results with notorious ambiguity, such as over-smoothed facial details and distorted contours.

As analyzed in Sec. I, directly utilizing SotA face SR and inpainting methods fails to solve this challenging problem. Therefore, the results of SR+PA and PA+SR methods suffer from corrupted facial regions and ghosting artifacts (see Figs. 5(c)-(h)).

Since FCSR-GAN super-resolves and inpaints occluded LR faces in an integrated framework, it avoids exaggerating errors

TABLE II: Ablation study of facial geometry priors.

	CelebA-HQ		Multi-PIE	
	PSNR	SSIM	PSNR	SSIM
P-FP	21.739	0.648	19.325	0.602
P+GT	26.340	0.791	24.007	0.733
Pro-UIGAN	25.470	0.763	23.188	0.704

TABLE III: Ablation study of different training losses.

	CelebA-HQ		Multi-PIE	
	PSNR	SSIM	PSNR	SSIM
L_G^-	19.136	0.605	18.473	0.579
L_G^+	20.872	0.628	19.281	0.610
L_G^\dagger	22.359	0.664	20.403	0.619
L_G^*	24.960	0.756	22.755	0.674
L_G	25.470	0.763	23.188	0.704

caused by model combination and generates relatively satisfying results. However, FCSR-GAN is a single-stage model, which does not possess a “looking back” ability to revise upsampled HR faces. Consequently, when the input LR faces are under large poses or complex expressions (see Fig. 5(a)), FCSR-GAN produces blurry HR faces, as seen in Fig. 5(i).

As shown in Fig. 5(j), our Pro-UIGAN generates visually appealing non-occluded HR faces from very LR and occluded inputs. Specifically, we show challenging examples with extreme poses and expressions (*e.g.*, the first, third, and sixth lines in Fig. 5(a)). It demonstrates that the hallucinated faces of our Pro-UIGAN are more authentic and vivid. Pro-UIGAN exploits a multi-stage progressive hallucination strategy and thus refines the hallucinated faces gradually, thus achieving superior hallucination performance.

C. Quantitative Evaluation

To evaluate the hallucination performance quantitatively, we provide the average Peak Single-to-Noise Ratio (PSNR) and Structural Similarity (SSIM) values of all methods on the testing sets in Tab. I.

Tab. I shows that our Pro-UIGAN obtains the best quantitative results in comparison to the SotA methods on all the databases. For example, on the CelebA-HQ testing set, Pro-UIGAN surpasses the other baselines by improving the PSNR by 8.7% dB. This is mainly because our model progressively refines hallucinated results via a coarse-to-fine manner. Furthermore, Tab. I also indicates that inpainting followed by super-resolution leads to slightly higher quantitative results than super-resolution followed by inpainting. This implies that super-resolving non-occluded LR facial patterns are easier than occluded ones.

D. Ablation Analysis

1) *Impacts of facial geometry priors:* In our work, we exploit facial geometry priors, *i.e.*, facial landmark heatmaps, for joint face SR and inpainting. We give a full discussion about how many improvements the facial geometry priors bring.

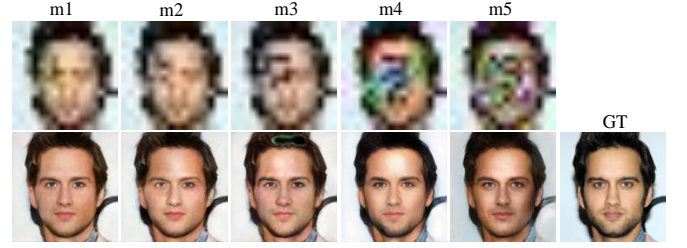


Fig. 6: Qualitative evaluation on different mask sizes.

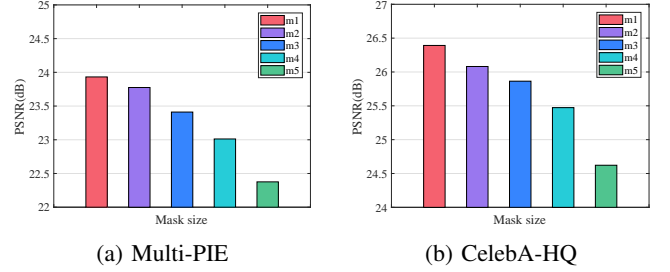


Fig. 7: Quantitative evaluation on different mask sizes.

We formulate two baseline models as below (we denote Pro-UIGAN as P, estimated facial priors as FP, and ground-truth facial priors as GT):

- P-FP: we discard the estimated facial priors of CM-TMs and employ the facial appearance features as the input of TUNs.
- P+GT: we use ground-truth facial landmark heatmaps instead of estimated facial priors, denoted by the “P+GT” model.

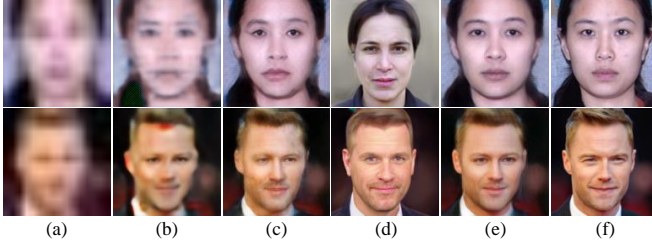
As illustrated in Fig. 4, the result of “P+GT” model (see Fig. 4(i)) shows more accurate facial geometry than the results of “P-FP” model (see Fig. 4(h)) and our Pro-UIGAN (see Fig. 4(l)). This implies the importance of facial geometry priors in the hallucination process: accurate facial prior knowledge assists in reducing the ambiguous mapping caused by occlusions and thus facilitates the upsampling procedures. As shown in Tab. II, the P+GT model (with the ground-truth facial geometry priors) outperforms the Pro-UIGAN model (with the estimated facial geometry prior) and P-FP model (without prior information) with the PSNR improvement of 0.819 dB and 4.682 dB on CelebA-HQ, respectively. Consequently, facial geometry priors significantly promote the model performance and thus achieve high-quality hallucinated results.

2) *Impact of different losses:* We provide the results of our Pro-UIGAN trained by using different losses on Multi-PIE and CelebA-HQ (see Tab. III and Fig. 4). We denote the compared Pro-UIGAN variants as follows: (i) L_G^- : L_{mse} and L_h ; (ii) L_G^+ : L_{mse} , L_{id} , and L_h ; (iii) L_G^\dagger : L_{mse} , L_{id} , L_h , and L_{sys} ; (iv) L_G^* : L_{mse} , L_{id} , L_h , L_{sys} , L_{style} , and L_{adv}^l ; (v) L_G : L_{mse} , L_{id} , L_h , L_{sys} , L_{style} , L_{adv}^l , and L_{adv}^g . Note that L_h is a prerequisite constraint in training our CM-TMs.

Fig. 4(f) shows that only exploiting the intensity similarity loss L_{mse} results in overly smooth results. Therefore, we introduce an identity similarity loss L_{id} to improve the visual quality (see Fig. 4(f)). The same results are confirmed by

TABLE IV: Efficiency comparisons on the CelebA-HQ testing set.

Method		Model Size (KB)	Running Time (ms)	PSNR (dB)
PA+SR SR+PA	FSRnet [7]	69,200	286.08	16.445/15.011
	FHC [3]	71,700	289.12	19.224/16.950
	PULSE [9]	118,500	5128.36	15.270/13.106
Joint SR+PA	FCSR-GAN [4]	112,200	145.69	23.010
	Pro-UIGAN	42,000	34.21	25.470

Fig. 8: Comparisons with SotA face SR methods. Columns: (a) Non-occluded LR inputs (16×16 pixels). (b) FSRnet [7]. (c) FHC [3]. (d) PULSE [9]. (e) Ours. (f) Ground-truth HR images (128×128 pixels).

the quantitative results in Tab. III (*i.e.*, L_G^- and L_G^\dagger). To guarantee the content integrity of completed faces, the mirror symmetry loss L_{sys} is employed for training our network. L_{sys} reduces the reconstruction errors during the training procedure and improves the model performance (see L_G^\dagger in Tab. III). Furthermore, as indicated in Tab. III (L_G^\dagger) and Fig. 4(k), the Local-D improves the model performance. However, the face in Fig. 4(k) still suffers from global structural inconsistency. Finally, after incorporating Global-D, Pro-UIGAN achieves the most satisfying faces (see Fig. 4(l)) and the best quantitative results (L_G in Tab. III).

E. Impacts of Different Mask Sizes

We evaluate the impact of different mask sizes on our model. The compared masks are as follows: (a) m1: 16×16 , (b) m2: 24×24 , (c) m3: 32×32 , (d) m4: 48×48 , (e) m5: 64×64 .

Figs. 6 and 7 show the qualitative and quantitative results of LR faces with different masks. The performance of our Pro-UIGAN gradually drops when the mask size increases. This is expected as larger mask sizes indicate more uncertain pixel values. But generally, our Pro-UIGAN performs well for all mask sizes, even when the occluded region is with a large size (*i.e.*, m5). Our facial geometry priors ensure the integrity of the facial structure and the consistency of facial attributes for the generated results, thus ensuring satisfying inpainting performance.

F. Efficiency Analysis

We provide efficiency comparisons for our Pro-UIGAN and the competing baselines in Tab. IV. Compared with the SotA methods, our Pro-UIGAN requires the shortest running time

(34.21 ms) because Pro-UIGAN performs face SR and inpainting seamlessly. Moreover, despite our multi-stage framework, Pro-UIGAN is more lightweight than the compared models. Note that we achieve the best quantitative results as indicated by the PSNR in Tab. IV. As a result, our Pro-UIGAN model is computationally efficient and functionally prominent.

G. Facial Attributes Manipulation

After hallucinating the occluded LR faces, users may not be satisfied with the generated facial attributes and want to manipulate them. We demonstrate that our model allows the users to conduct interactive facial attribute editing on the hallucinated face. As shown in Fig. 9, we can change the facial geometry priors to modify one attribute (*i.e.*, mouth, nose, or eyes) while other attributes are maintained similar to the ground-truth.

H. Performance on Non-occluded LR Faces

As illustrated in Fig. 1(d), the face inpainting method [2] fails to inpaint LR faces and produces inferior results. Then, the errors would be exaggerated in the following face SR process (see Fig. 1(f)). In contrast, we jointly inpaint and super-resolve occluded LR faces rather than tackling these two tasks separately. Hence, we alleviate the side-effects of direct model combination.

For fair comparisons, we conduct experiments to evaluate Pro-UIGAN and SotA face SR methods on non-occluded LR faces. In this case, face inpainting methods are not indispensable and thereby not employed. According to the results in Fig. 8, Pro-UIGAN still outperforms the SotA methods and achieves more visually appealing and identity-preserving results. This demonstrates the effectiveness of our progressive learning strategy and the identity-preserving ability of our model.

I. Performance on Faces with Real Occlusions

We demonstrate our method can effectively hallucinate the faces where real occlusions occur. We select a few CelebA-HQ testing faces partly occluded by objects such as glasses or microphones. Since such regions in the images are occluded or not is subjective, we give users this option to appoint the occluded regions through appending masks. Then, we obtain the occluded LR faces (16×16 pixels) by transforming and downsampling the processed images. As shown in Fig. 10, our model not only hallucinates the visually appealing HR faces but also removes the real occlusions. Furthermore, we present the cosine distances between LR faces, hallucinated HR faces, and their ground-truths (see Fig. 10). Here, we employ a SotA pre-trained face recognition model (ArcFaceNet [53]) to extract the deep features for calculation. As a result, our Pro-UIGAN reconstructs face images with high-fidelity identity information, in comparison to the SotA [4].

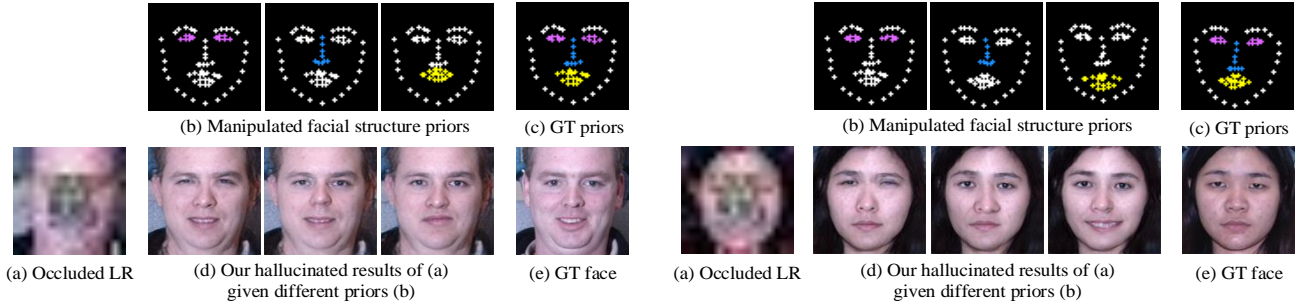


Fig. 9: Facial attribute editing results.

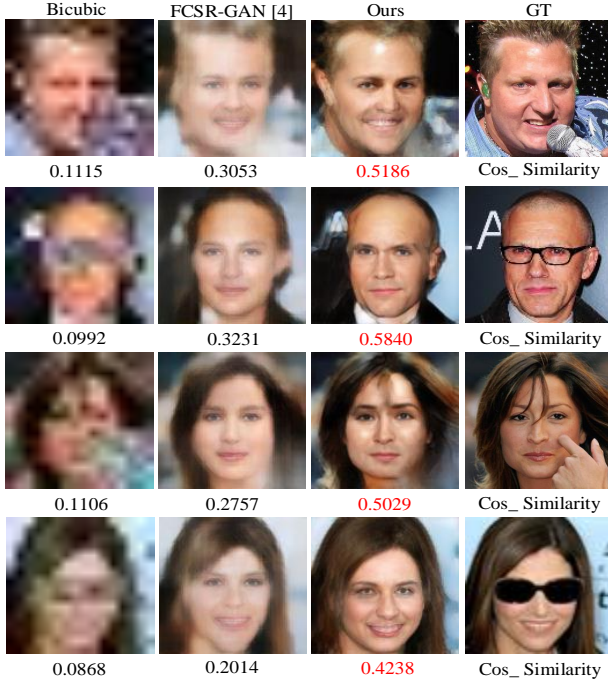


Fig. 10: Face hallucination results of real occlusions.

V. FACE HALLUCINATION EVALUATION VIA DOWNSTREAM TASKS

A. Comparisons with SotA on Face Alignment

We demonstrate that our Pro-UIGAN boosts the performance of low-quality face alignment. We adopt the “alignment via hallucination” framework to conduct experiments on the **CelebA-HQ**, **Multi-PIE**, and **Helen** databases. Specifically, occluded LR faces are hallucinated by compared methods first and then used for alignment.

Fig. 11 shows the hallucinated images of compared methods and the facial landmarks estimated by FAN [29] on different hallucinated faces. Moreover, Tab. IV provides the NRMSE performance, which is a commonly used metric in face alignment. The results indicate that: (1) It is a challenge for SotA face alignment models to predict landmarks directly from occluded LR face images. The predicted landmarks of the bicubic face suffer from significant errors around the eyes, mouth, or noses. However, our Pro-UIGAN can alleviate the alignment difficulty and thus results in lower NRMSE values than bicubic faces (see Tab. V). (2) In comparison with FCSR-GAN [4],

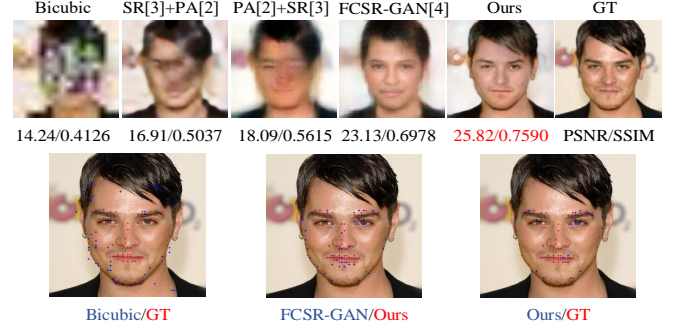


Fig. 11: Qualitative comparisons of face alignment.

our hallucinated face provides visually superior estimation on facial components and shapes, achieving the lowest NRMSE values on all datasets. These results demonstrate that Pro-UIGAN reconstructs facial geometry more accurately and is practical for low-quality face alignment tasks.

B. Comparisons with SotA on Face Parsing

We manifest that our Pro-UIGAN also benefits low-quality face parsing tasks. Similarly, we adopt an off-the-shelf face parsing model [1] to conduct face parsing experiments for recovered images of compared methods.

As shown in Fig. 12, the parsing maps of our hallucinated face images separate complete and accurate facial components, while others provide wrong shapes or lose components (*i.e.*, eyes, nose, or mouth). Meanwhile, we report the Intersection-over-Union (IoU) results on the testing sets with comparisons to the SotA (see Tab. V). As shown in Tab. V, our Pro-UIGAN yields the highest parsing accuracy and surpasses the competing methods by a large margin (over 5%) in terms of IoU on all databases. The comparison implies that Pro-UIGAN is a better method to reconstruct semantic-level facial features, thus positively affecting low-quality face parsing.

C. Comparisons with SotA on Face Recognition

The cosine distances in Fig. 12 partly reveal the identity-preserving ability of our model. In this section, we conduct face recognition experiments to discuss how much the face identity information can be preserved. This task simulates an open problem: occluded and low-resolution face recognition.

TABLE V: Quantitative comparisons on face alignment (NRMSE) and face parsing (IoU).

SR Method	CelebA-HQ		Multi-PIE		Helen		CelebA-HQ		Multi-PIE		Helen	
	SR+PA [2]						PA [2]+SR					
	NRMSE	IoU	NRMSE	IoU	NRMSE	IoU	NRMSE	IoU	NRMSE	IoU	NRMSE	IoU
Bicubic	30.67	0.0071	33.21	0.0074	35.64	0.0076	27.31	0.0076	29.56	0.0083	32.33	0.0082
FSRnet [7]	22.03	0.3484	24.68	0.3233	26.11	0.3192	20.13	0.3609	22.31	0.3404	23.74	0.3326
FHC [3]	18.35	0.4153	20.11	0.4049	20.87	0.3990	16.57	0.4318	17.32	0.4229	18.26	0.4166
PULSE [9]	40.07	0.1740	52.08	0.0646	44.35	0.1069	38.79	0.1834	49.22	0.0718	40.13	0.1261
FCSR-GAN [4]	9.74	0.5445	10.57	0.5231	11.69	0.4870	9.74	0.5445	10.57	0.5231	11.69	0.4870
Pro-UIGAN	7.31	0.6008	8.34	0.5822	9.96	0.5633	7.31	0.6008	8.34	0.5822	9.96	0.5633
Ground-truth HR	4.27	0.6501	2.58	None	3.84	0.6056	4.27	0.6501	2.58	None	3.84	0.6056

For Multi-PIE, parsing maps from ground-truth HR images are used as ground-truths.

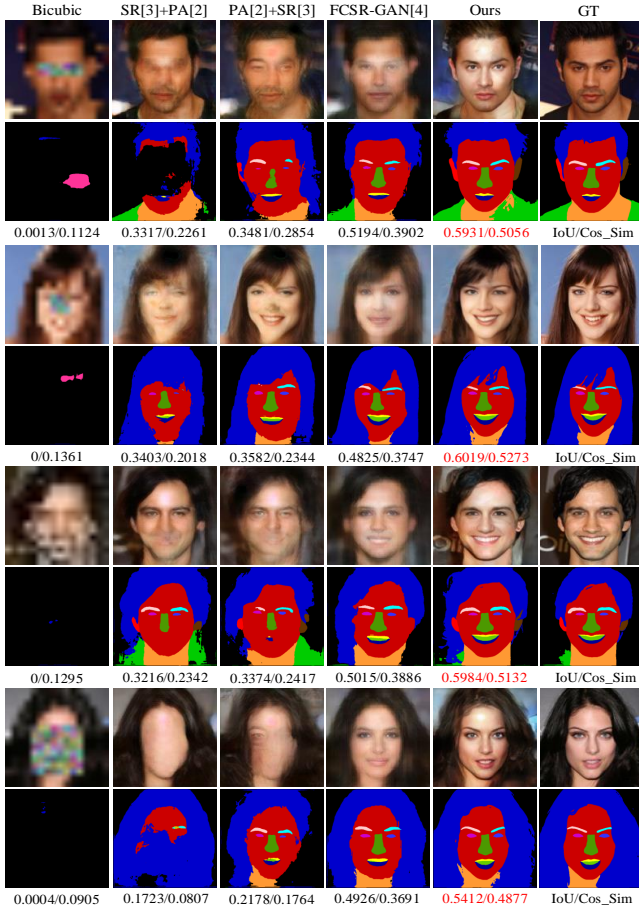


Fig. 12: Qualitative comparisons of face parsing.

1) *Experimental settings*: We use the “recognition via hallucination” scheme to conduct experiments on **Multi-PIE** [50]. First, we split the Multi-PIE face images according to the identity ID and construct subject disjoint training and testing sets. Then, we train the competing methods on the training set and conduct face recognition experiments on the testing set. Here, we choose the frontal HR face images of testing individuals to form our testing set. We apply the four masking types in Fig. 12 for each HR face. These masking types simulate the most common occlusions in the real world. For example, masking mouths simulates wearing masks, and masking eyes

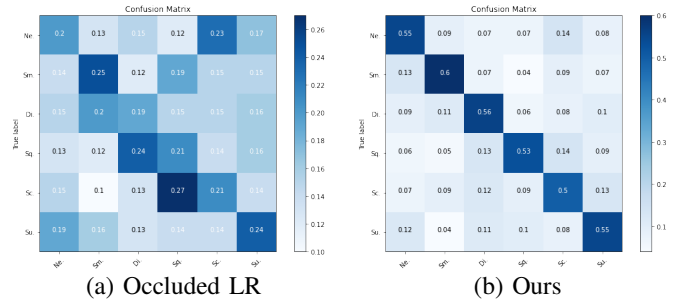


Fig. 13: Face recognition results for compared methods on Multi-PIE.

simulates wearing glasses. Subsequently, we generate occluded LR faces by downsampling and transforming the masked HR ones. Finally, we use a SotA pre-trained face recognition model [53] to conduct face recognition experiments on occluded LR faces and hallucinated non-occluded HR faces generated by compared methods.

2) *Evaluation*: As shown Fig. 13, the face recognition rate of our hallucinated faces outperforms those of the occluded LR faces and the compared methods’ results. This demonstrates that our Pro-UIGAN possesses significant identity preservation ability and benefits low-quality face recognition tasks.

D. Comparisons with SotA on Face Expression Classification

We demonstrate that Pro-UIGAN can preserve facial expressions and boost the performance of low-quality face expression classification.

1) *Experimental settings*: We conduct a standard 10-fold subject-independent cross-validation [54], [55] on **Multi-PIE** [50]. First, we split the synthesized occluded LR/non-occluded HR Multi-PIE face pairs according to the identity ID and form 10 subject-independent subsets. Then, we conduct ten-fold validation experiments. In each experiment, we choose 9 subsets to construct the training set and the remaining one to form the testing set. The compared face hallucination models are first trained on the same training set and then used to upsample and inpaint the testing faces. We introduce a SotA expression classification model [45] to classify the facial expression of hallucinated faces. Finally, for each compared method, we calculate the average of the

TABLE VI: Face expression classification results for compared methods on Multi-PIE

SR method	Accuracy	
	PA+SR	SR+PA
Bicubic	22.34%	20.59%
FSRnet [7]	24.07%	22.52%
PULSE [9]	27.40%	24.16%
FHC [3]	30.66%	28.31%
FCSR-GAN [4]	45.93%	
Occluded LR	22.14%	
Non-occluded HR	94.62%	
Pro-UIGAN	55.57%	

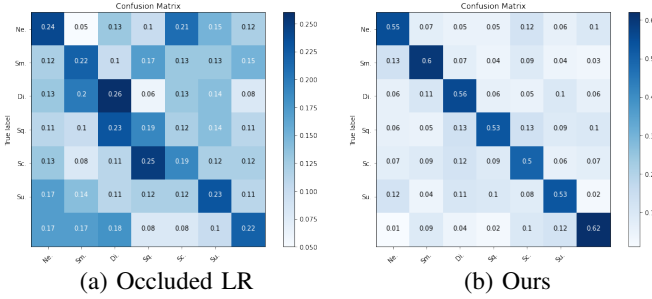


Fig. 14: The confusion matrices of LR faces and our hallucinated ones. Darker colors indicate higher accuracy.

expression classification results of the 10 subsets. Here, we set the classification results of the occluded LR faces and the non-occluded HR ones as the lower and upper bounds for this task (see Tab. VI).

2) *Evaluation*: As shown in Tab. VI, the non-occluded HR faces hallucinated by our Pro-UIGAN achieve superior expression classification accuracy in comparison to the SotA. Meanwhile, we provide the confusion matrix for occluded LR faces and our hallucinated ones (see Fig. 14). It can be observed that the faces hallucinated by Pro-UIGAN outperform occluded-LR ones on all the expressions. These results indicate that Pro-UIGAN recovers authentic facial expressions and benefits low-quality face expression classification tasks.

VI. CONCLUSION

This paper presents a Pro-UIGAN framework to jointly super-resolve and inpaint occluded LR face images seamlessly. Moreover, our developed multi-stage progressive learning strategy allows us to achieve coarse-to-fine feature refinement under the guidance of facial geometry priors. Meanwhile, we provide a solution to estimating facial landmarks from occluded thumbnails, thus significantly improving our hallucination performance. Experimental results on multiple widely-used benchmarks confirm the efficacy of Pro-UIGAN in generating identity-preserving face images and substantially benefiting downstream tasks.

REFERENCES

[1] S. Liu, J. Yang, C. Huang, and M.-H. Yang, “Multi-objective convolutional learning for face labeling,” in *The IEEE Conference on Computer Vision and Pattern Recognition (CVPR)*, June 2015.

[2] Y. Li, S. Liu, J. Yang, and M.-H. Yang, “Generative face completion,” in *Proceedings of the IEEE conference on computer vision and pattern recognition*, 2017, pp. 3911–3919.

[3] X. Yu, B. Fernando, B. Ghanem, F. Porikli, and R. Hartley, “Face super-resolution guided by facial component heatmaps,” in *Proceedings of European Conference on Computer Vision (ECCV)*, 2018, pp. 217–233.

[4] J. Cai, H. Han, S. Shan, and X. Chen, “Fcsr-gan: Joint face completion and super-resolution via multi-task learning,” *IEEE Transactions on Biometrics, Behavior, and Identity Science*, vol. 2, no. 2, pp. 109–121, 2019.

[5] S. Zhu, S. Liu, C. C. Loy, and X. Tang, “Deep cascaded bi-network for face hallucination,” in *Proceedings of European Conference on Computer Vision (ECCV)*, 2016, pp. 614–630.

[6] Q. Cao, L. Lin, Y. Shi, X. Liang, and G. Li, “Attention-aware face hallucination via deep reinforcement learning,” in *Proceedings of the IEEE Conference on Computer Vision and Pattern Recognition (CVPR)*, 2017, pp. 690–698.

[7] Y. Chen, Y. Tai, X. Liu, C. Shen, and J. Yang, “Fsrnet: End-to-end learning face super-resolution with facial priors,” in *Proceedings of the IEEE Conference on Computer Vision and Pattern Recognition (CVPR)*, 2018, pp. 2492–2501.

[8] X. Yu and F. Porikli, “Imagining the unimaginable faces by deconvolutional networks,” *IEEE Transactions on Image Processing*, vol. 27, no. 6, pp. 2747–2761, 2018.

[9] S. Menon, A. Damian, S. Hu, N. Ravi, and C. Rudin, “Pulse: Self-supervised photo upsampling via latent space exploration of generative models,” in *Proceedings of the IEEE/CVF conference on computer vision and pattern recognition*, 2020, pp. 2437–2445.

[10] L. Song, J. Cao, L. Song, Y. H. Hu, and R. He, “Geometry-aware face completion and editing,” 2019.

[11] X. Wang and X. Tang, “Hallucinating face by eigentransformation,” *IEEE Transactions on Systems, Man, and Cybernetics, Part C (Applications and Reviews)*, vol. 35, no. 3, pp. 425–434, 2005.

[12] C. Liu, H.-Y. Shum, and W. T. Freeman, “Face hallucination: Theory and practice,” *International Journal of Computer Vision*, vol. 75, no. 1, pp. 115–134, 2007.

[13] S. Kolouri and G. K. Rohde, “Transport-based single frame super resolution of very low resolution face images,” in *Proceedings of the IEEE Conference on Computer Vision and Pattern Recognition (CVPR)*, 2015, pp. 4876–4884.

[14] X. Ma, J. Zhang, and C. Qi, “Hallucinating face by position-patch,” *Pattern Recognition*, vol. 43, no. 6, pp. 2224–2236, 2010.

[15] J. Jiang, R. Hu, Z. Wang, and Z. Han, “Face super-resolution via multi-layer locality-constrained iterative neighbor embedding and intermediate dictionary learning,” *IEEE Transactions on Image Processing*, vol. 23, no. 10, pp. 4220–4231, 2014.

[16] Y. Li, C. Cai, G. Qiu, and K.-M. Lam, “Face hallucination based on sparse local-pixel structure,” *Pattern Recognition*, vol. 47, no. 3, pp. 1261–1270, 2014.

[17] R. A. Farrugia and C. Guillemot, “Face hallucination using linear models of coupled sparse support,” *IEEE Transactions on Image Processing*, vol. 26, no. 9, pp. 4562–4577, 2017.

[18] L. Liu, C. P. Chen, S. Li, Y. Y. Tang, and L. Chen, “Robust face hallucination via locality-constrained bi-layer representation,” *IEEE Transactions on Cybernetics*, vol. 48, no. 4, pp. 1189–1201, 2017.

[19] M. F. Tappen and C. Liu, “A bayesian approach to alignment-based image hallucination,” in *Proceedings of European Conference on Computer Vision (ECCV)*, 2012, pp. 236–249.

[20] C.-Y. Yang, S. Liu, and M.-H. Yang, “Hallucinating compressed face images,” *International Journal of Computer Vision*, vol. 126, no. 6, pp. 597–614, 2018.

[21] X. Yu and F. Porikli, “Ultra-resolving face images by discriminative generative networks,” in *Proceedings of European Conference on Computer Vision (ECCV)*, 2016, pp. 318–333.

[22] H. Huang, R. He, Z. Sun, and T. Tan, “Wavelet domain generative adversarial network for multi-scale face hallucination,” *International Journal of Computer Vision*, vol. 127, no. 6–7, pp. 763–784, 2019.

[23] X. Yu and F. Porikli, “Face hallucination with tiny unaligned images by transformative discriminative neural networks,” in *Thirty-First AAAI Conference on Artificial Intelligence*, 2017, p. 4327–4333.

[24] X. Xu, D. Sun, J. Pan, Y. Zhang, H. Pfister, and M.-H. Yang, “Learning to super-resolve blurry face and text images,” in *Proceedings of International Conference on Computer Vision (ICCV)*, 2017, pp. 251–260.

[25] R. Dahl, M. Norouzi, and J. Shlens, “Pixel recursive super resolution,” in *Proceedings of International Conference on Computer Vision (ICCV)*, 2017, pp. 5439–5448.

- [26] A. V. Oord, N. Kalchbrenner, and K. Kavukcuoglu, "Pixel recurrent neural networks," in *Proceedings of Machine Learning Research*, vol. 48, 2016, pp. 1747–1756.
- [27] X. Yu, F. Porikli, B. Fernando, and R. Hartley, "Hallucinating unaligned face images by multiscale transformative discriminative networks," *International Journal of Computer Vision*, pp. 1–27, 2019.
- [28] Y. Zhang, I. W. Tsang, Y. Luo, C.-H. Hu, X. Lu, and X. Yu, "Copy and paste gan: Face hallucination from shaded thumbnails," in *Proceedings of the IEEE/CVF Conference on Computer Vision and Pattern Recognition*, 2020, pp. 7355–7364.
- [29] A. Bulat and G. Tzimiropoulos, "How far are we from solving the 2d & 3d face alignment problem?(and a dataset of 230,000 3d facial landmarks)," in *Proceedings of International Conference on Computer Vision (ICCV)*, 2017, pp. 1021–1030.
- [30] M. Bertalmio, G. Sapiro, V. Caselles, and C. Ballester, "Image inpainting," in *Proceedings of the 27th annual conference on Computer graphics and interactive techniques*, 2000, pp. 417–424.
- [31] M. Elad, J.-L. Starck, P. Querre, and D. L. Donoho, "Simultaneous cartoon and texture image inpainting using morphological component analysis (mca)," *Applied and Computational Harmonic Analysis*, vol. 19, no. 3, pp. 340–358, 2005.
- [32] S. Darabi, E. Shechtman, C. Barnes, D. B. Goldman, and P. Sen, "Image melding: Combining inconsistent images using patch-based synthesis," *ACM Transactions on graphics (TOG)*, vol. 31, no. 4, pp. 1–10, 2012.
- [33] M. Bertalmio, L. Vese, G. Sapiro, and S. Osher, "Simultaneous structure and texture image inpainting," *IEEE transactions on image processing*, vol. 12, no. 8, pp. 882–889, 2003.
- [34] A. Criminisi, P. Pérez, and K. Toyama, "Region filling and object removal by exemplar-based image inpainting," *IEEE Transactions on image processing*, vol. 13, no. 9, pp. 1200–1212, 2004.
- [35] J. Hays and A. A. Efros, "Scene completion using millions of photographs," *ACM Transactions on Graphics (ToG)*, vol. 26, no. 3, pp. 4-es, 2007.
- [36] D. Pathak, P. Krahenbuhl, J. Donahue, T. Darrell, and A. A. Efros, "Context encoders: Feature learning by inpainting," in *Proceedings of the IEEE conference on computer vision and pattern recognition*, 2016, pp. 2536–2544.
- [37] S. Iizuka, E. Simo-Serra, and H. Ishikawa, "Globally and locally consistent image completion," *ACM Transactions on Graphics (ToG)*, vol. 36, no. 4, pp. 1–14, 2017.
- [38] S. Zhang, R. He, Z. Sun, and T. Tan, "Demeshnet: Blind face inpainting for deep meshface verification," *IEEE Transactions on Information Forensics and Security*, vol. 13, no. 3, pp. 637–647, 2017.
- [39] P. Liu, X. Qi, P. He, Y. Li, M. R. Lyu, and I. King, "Semantically consistent image completion with fine-grained details," *arXiv preprint arXiv:1711.09345*, 2017.
- [40] T. Zhou, C. Ding, S. Lin, X. Wang, and D. Tao, "Learning oracle attention for high-fidelity face completion," in *Proceedings of the IEEE/CVF Conference on Computer Vision and Pattern Recognition*, 2020, pp. 7680–7689.
- [41] Y. Bengio, J. Louradour, R. Collobert, and J. Weston, "Curriculum learning," in *Proceedings of the 26th annual international conference on machine learning*, 2009, pp. 41–48.
- [42] K. He, X. Zhang, S. Ren, and J. Sun, "Deep residual learning for image recognition," in *Proceedings of the IEEE Conference on Computer Vision and Pattern Recognition (CVPR)*, 2016, pp. 770–778.
- [43] C. Ledig, L. Theis, F. Huszár, J. Caballero, A. Cunningham, A. Acosta, A. Aitken, A. Tejani, J. Totz, Z. Wang *et al.*, "Photo-realistic single image super-resolution using a generative adversarial network," in *Proceedings of the IEEE Conference on Computer Vision and Pattern Recognition (CVPR)*, 2017, pp. 4681–4690.
- [44] F. Shiri, X. Yu, F. Porikli, R. Hartley, and P. Koniusz, "Identity-preserving face recovery from stylized portraits," *International Journal of Computer Vision*, vol. 127, no. 6-7, pp. 863–883, 2019.
- [45] K. Simonyan and A. Zisserman, "Very deep convolutional networks for large-scale image recognition," in *Proceedings of International Conference on Learning Representations (ICLR)*, 2015, pp. 1–14.
- [46] Y. Zhang, I. W. Tsang, J. Li, P. Liu, X. Lu, and X. Yu, "Face hallucination with finishing touches," *IEEE Transactions on Image Processing*, vol. 30, pp. 1728–1743, 2021.
- [47] X. Yu, B. Fernando, R. Hartley, and F. Porikli, "Super-resolving very low-resolution face images with supplementary attributes," in *Proceedings of the IEEE Conference on Computer Vision and Pattern Recognition (CVPR)*, 2018, pp. 908–917.
- [48] G. Liu, F. A. Reda, K. J. Shih, T.-C. Wang, A. Tao, and B. Catanzaro, "Image inpainting for irregular holes using partial convolutions," in *Proceedings of the European Conference on Computer Vision (ECCV)*, 2018, pp. 85–100.
- [49] Z. Liu, P. Luo, X. Wang, and X. Tang, "Deep learning face attributes in the wild," in *Proceedings of International Conference on Computer Vision (ICCV)*, December 2015, p. 3730–3738.
- [50] R. Gross, I. Matthews, J. Cohn, T. Kanade, and S. Baker, "Multi-pie," *Image and Vision Computing*, vol. 28, no. 5, pp. 807–813, 2010.
- [51] V. Le, J. Brandt, Z. Lin, L. Bourdev, and T. S. Huang, "Interactive facial feature localization," in *European conference on computer vision*. Springer, 2012, pp. 679–692.
- [52] T. Karras, T. Aila, S. Laine, and J. Lehtinen, "Progressive growing of gans for improved quality, stability, and variation," *arXiv preprint arXiv:1710.10196*, 2017.
- [53] W. Liu, Y. Wen, Z. Yu, M. Li, B. Raj, and L. Song, "Sphereface: Deep hypersphere embedding for face recognition," in *Proceedings of the IEEE Conference on Computer Vision and Pattern Recognition (CVPR)*, 2017.
- [54] P. Liu, S. Han, Z. Meng, and Y. Tong, "Facial expression recognition via a boosted deep belief network," in *Proceedings of the IEEE Conference on Computer Vision and Pattern Recognition (CVPR)*, 2014, pp. 1805–1812.
- [55] P. Liu, J. T. Zhou, I. W.-H. Tsang, Z. Meng, S. Han, and Y. Tong, "Feature disentangling machine-a novel approach of feature selection and disentangling in facial expression analysis," in *Proceedings of European Conference on Computer Vision (ECCV)*. Springer, 2014, pp. 151–166.

Pro-UIGAN: Progressive Face Hallucination from Occluded Thumbnails

Yang Zhang, Xin Yu, Xiaobo Lu, Ping Liu

Abstract—In this paper, we study the task of hallucinating an authentic high-resolution (HR) face from an occluded thumbnail. We propose a multi-stage Progressive Upsampling and Inpainting Generative Adversarial Network, dubbed Pro-UIGAN, which exploits facial geometry priors to replenish and upsample ($8\times$) the occluded and tiny faces (16×16 pixels). Pro-UIGAN iteratively (1) estimates facial geometry priors for low-resolution (LR) faces and (2) acquires non-occluded HR face images under the guidance of the estimated priors. Our multi-stage hallucination network upsamples and inpaints occluded LR faces via a coarse-to-fine fashion, significantly reducing undesirable artifacts and blurriness. Specifically, we design a novel cross-modal transformer module for facial priors estimation, in which an input face and its landmark features are formulated as queries and keys, respectively. Such a design encourages joint feature learning across the input facial and landmark features, and deep feature correspondences will be discovered by attention. Thus, facial appearance features and facial geometry priors are learned in a mutual promotion manner. Extensive experiments show that our Pro-UIGAN attains visually pleasing completed HR faces, thus facilitating downstream tasks, *i.e.*, face alignment, face parsing, face recognition as well as expression classification.

Index Terms—Face inpainting, super-resolution, face hallucination, generative adversarial network.

I. INTRODUCTION

With the increasing demand for social security, non-intrusive identity verification has become indispensable in daily life. As face is one of the most frequently utilized biometric cues, it is highly desirable to obtain face images in high quality in order to provide essential information for identity verification. However, in real scenarios, such as in surveillance systems, the captured faces usually not only are in low resolutions but also undergo occlusions caused by body parts or accessories, such as eye-glasses, scarves, etc. Since the information available in those low-resolution (LR) face images with occlusions is quite limited, it is difficult to extract useful features to support downstream applications, such as

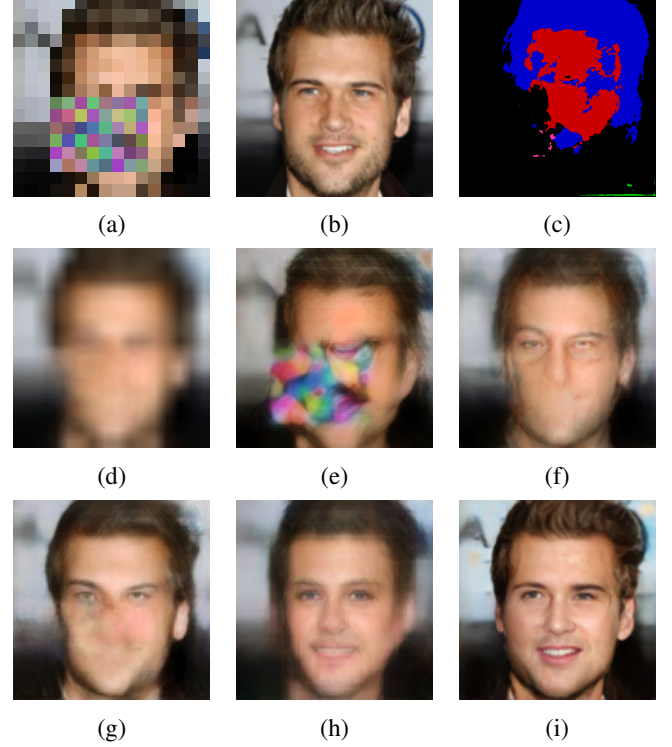


Fig. 1: Face inpainting and upsampling results on an occluded LR face. (a) The 16×16 occluded LR face image. (b) The original 128×128 non-occluded HR face image. (c) Face parsing result of (a), which is obtained by applying bicubic interpolation followed by the work [?]. (d) Face inpainting result of (a), which is obtained by applying bicubic interpolation followed by the work [?]. (e) Face SR result of (a) by applying [?]. (f) Result obtained by applying [?] followed by [?]. (g) Result obtained by applying [?] followed by [?]. (h) Result of FCSR-GAN [?]. (i) Result of our Pro-UIGAN.

face verification and facial attribute classification. Therefore, it becomes necessary to design advanced methods to hallucinate LR images and uncover the information from occlusions.

One straightforward solution to hallucinating LR face images with occlusions is directly utilizing existing face SR methods [?], [?], [?], [?], [?], [?] and face inpainting solutions [?], [?] to process the LR images with occlusions, which, however, has been experimentally proved sub-optimal. On the one hand, off-the-shelf face inpainting methods usually require a high-resolution (HR) face image as their inputs to analyze the context in facial regions. When the input images are in low

Y. Zhang is with the Key Laboratory of Intelligent Perception and Systems for High-Dimensional Information, Ministry of Education, School of Computer Science and Engineering, Nanjing University of Science and Technology, Nanjing 210094, China, e-mail: zhangyang201703@126.com.

X. Yu is with the Australian Institute of Artificial Intelligence, University of Technology Sydney, Ultimo, NSW 2007, Australia, e-mail: xin.yu@uts.edu.au.

X. B. Lu is with the School of Automation, Southeast University, Nanjing 210096, China; Key Laboratory of Measurement and Control of Complex Systems of Engineering, Ministry of Education, Nanjing 210096, China, e-mail: xblu2013@126.com.

P. Liu (corresponding author) is with the Institute of High Performance Computing, Research Agency for Science, Technology and Research (A*STAR), Singapore 138634, e-mail: pino.pingliu@gmail.com.

resolutions, for example, 16×16 pixels, it becomes impractical to accurately segment the facial areas (see Fig. 1(c)), let alone conducting further analysis and modeling on each facial component. Hence, inpainting leads to overly-blurred facial details (see Fig. 1(d)). Those errors might be exaggerated in the following face SR process (see Fig. 1(f)). On the other hand, most of existing face SR solutions only consider non-occluded face images as their inputs. These methods may suffer from ghosting artifacts in the results when LR inputs with occlusions are given (see Fig. 1(e)). Moreover, when we apply face inpainting methods on those hallucinated images, the final results will exhibit severe distortions (see Fig. 1(g)). Based on our observations, we believe that treating face SR and face inpainting as two independent tasks is not an ideal solution.

Very recently, [?] proposes a deep generative adversarial network (FCSR-GAN) to jointly super-resolve and inpaint occluded face images in low resolutions. Compared to the solutions which directly combine face inpainting and SR methods, FCSR-GAN is able to alleviate artifacts to some extent. However, FCSR-GAN may output blurry results when the inputs have very low resolutions and extreme poses. As shown in Fig. 1(h), over-smoothed facial details and severe distortions appear in the hallucinated face.

In this paper, we propose to hallucinate occluded LR inputs¹ while achieving non-occluded HR faces² in a unified framework. In this manner, these two tasks (*i.e.*, face SR and face inpainting) are addressed simultaneously and mutually facilitate each other. Moreover, we design a progressive joint face SR and face inpainting framework, dubbed Pro-UIGAN. Pro-UIGAN runs in a multi-stage manner where each stage refines the face images hallucinated at the previous stage. By iteratively refining the details of hallucinated images, we can achieve high-quality results for large upsampling factors. Not only that, equipped with a delicate designed cross-modal attention mechanism, we exploit facial geometry priors (*i.e.*, facial landmark heatmaps) as the semantic guidance during our progressive hallucination process to reconstruct more realistic facial details.

Our Pro-UIGAN consists of a Pro-UI-net and two discriminators, *i.e.*, a local discriminator (namely Local-D) and a global discriminator (namely Global-D). The Pro-UI-net stacks a few successive Upsampling and Inpainting Blocks (UI-blocks) and generates a non-occluded HR face image by performing multiple inpainting and upsampling of an occluded LR face. By doing so, we can inpaint and super-resolve the LR input in a coarse-to-fine manner. In particular, in each stage, our UI-block comprises a Cross-modal Transformer Module (CM-TM) and a Transformative Upsampling Net (TUN). It estimates the most distinguishable facial landmarks in an input face and constructs facial geometry priors to guide hallucination. Our designed CM-TM employs the input face and its landmark features as queries and keys to calculate their cross-attention matrix for deep feature correspondences construction. Then, it generates facial geometry priors and facial appearance

features in a mutual promotion manner. In our multi-stage hallucination process, the first UI-block generates a coarse hallucinated face from the occluded LR input, which acts as a preliminary result for following UI-blocks. Then, the following UI-blocks refine the face images hallucinated at the previous stage and generate hallucination results with finer details. Fig. 1(i) illustrates that our hallucinated non-occluded HR face is more photo-realistic than the results of the state-of-the-art.

Overall, our contributions are fourfold:

- We present a novel framework, namely Progressive Upsampling and Inpainting Generative Adversarial Network (Pro-UIGAN), to jointly achieve face inpainting and face SR in a unified framework.
- We design a multi-stage hallucination and inpainting interwoven strategy. Specifically, we upsample and inpaint occluded LR faces via a coarse-to-fine fashion, thereby reducing undesirable artifacts and noises compared to a direct combination of face hallucination and inpainting methods.
- We propose a Cross-Modal Transformer Module (CM-TM) to collaboratively learn facial geometry priors and facial appearance features. Our CM-TM provides effective clues for feature alignment and enhancement, and thus promotes more accurate face hallucination results.
- Extensive experiments manifest that Pro-UIGAN authentically replenishes ($8\times$ upsampling) occluded and low-resolution face images (*i.e.*, 16×16 pixels). Moreover, our Pro-UIGAN provides superior hallucinated face images for downstream tasks, *i.e.*, face alignment, face parsing, face recognition as well as expression classification, in comparison to the SotA.

II. RELATED WORK

A. Face Super-resolution

Face Super-resolution (SR) aims at enhancing the resolution of LR face images to generate corresponding HR face images. The previous works can be generally grouped into three categories: holistic-based [?], [?], [?], part-based [?], [?], [?], [?], [?], [?], as well as deep learning based solutions [?], [?], [?], [?], [?], [?], [?], [?], [?].

Holistic-based methods employ global face models to up-sample LR faces. Wang *et al.* [?] establish a linear mapping between LR and HR images to achieve face SR based on an Eigen-transformation of LR faces. Liu *et al.* [?] incorporate a bilateral filtering to mitigate the ghosting artifacts, improving the quality of generated HR faces. Kolouri and Rohde [?] introduce optimal transport and subspace learning to morph HR faces from aligned LR ones. However, they require LR inputs to be precisely aligned, and reference HR faces are under canonical poses and natural expressions.

To handle large poses and complex expressions, part-based methods have been proposed to super-resolve local facial regions rather than enforcing global constraints. The works [?], [?], [?], [?] incorporate facial patches extracted from HR datasets to enhance input LR facial regions. Marshall *et al.* [?] employ the SIFT Flow algorithm to warp exemplar faces and

¹occluded LR faces: low-resolution faces with occlusions.

²non-occluded HR faces: high-resolution faces without occlusions.

compute the hallucinated HR image through MAP estimation. Yang *et al.* [?] use facial landmarks to retrieve adequate high-resolution facial component exemplars for further face super-resolution. Those works [?], [?] need to precisely localize facial components for face super-resolution, which is challenging, especially in LR cases.

Benefiting from the strong feature extraction ability of deep neural networks, deep learning-based solutions achieve promising performance compared to traditional techniques. Yu *et al.* [?] design a GAN-based model to upsample LR faces. Huang *et al.* [?] introduce wavelet coefficients into CNNs to super-resolve LR faces with multiple upscaling factors. Cao *et al.* [?] put forward an attention-aware mechanism and a local enhancement network to progressively enhance local facial regions during hallucination. Xu *et al.* [?] exploit a multi-class adversarial loss to promote joint face SR and deblurring. Dahl *et al.* [?] propose to super-resolve pre-aligned LR inputs via designing an autoregressive Pixel-RNN [?]. Yu *et al.* [?] incorporate facial component information from the intermediate upsampled features into an upsampling stream to achieve superior face hallucination results. Yu *et al.* [?] present a multiscale transformative discriminative neural network to super-resolve unaligned and very small faces of variable resolutions. Zhang *et al.* [?] present a two-branch upsampling framework to normalize and super-resolve non-uniform illumination and low-resolution inputs. Menon *et al.* [?] present a Photo Upsampling via Latent Space Exploration (PULSE) algorithm to generate high-quality frontal face images at large resolutions. Since those works [?], [?], [?], [?], [?], [?], [?], [?], [?], [?] aim to super-resolve LR faces without occlusions, they might obtain inferior results when occluded LR inputs are given, as seen in Fig. 1(e).

B. Image Inpainting

Image inpainting is to generate missing regions in corrupted images. The inpainted images should be not only visually realistic but also consistent in content. Image inpainting techniques can be divided into three categories. The first category employs the diffusion equation to iteratively propagate low-level features from the content area to the missing region along the boundaries [?], [?]. The methods belonging to the second category are patch-based methods, which search similar patches from the same image or exemplar image databases to fill in the missing contents [?], [?], [?], [?]. The third category is learning-based methods, which employ encoder-decoder networks to extract image features and generate missing content according to the extracted features [?], [?]. However, these methods generally focus on inpainting natural images rather than class-specific images, such as faces.

Face inpainting is even more challenging because the face topological structure and the face identity should be retained during the inpainting process and humans are very sensitive to distorted facial structure. In general, researchers usually introduce facial prior information to inpainting. S. Zhang *et al.* [?] aim to recover face images from structural obstructions such as streaks. However, their method is more effective when only a small area is missing. Li *et al.* [?] propose

a face inpainting GAN which introduces facial geometry as semantic regularization to maintain face topological structure. Meanwhile, they use both global and local discriminators to ensure the quality of completed face images. However, their algorithm is sensitive to pose and expression variations and may fail when the occluded faces are in low resolutions. [?] designs a geometry-aware face inpainting model which exploits facial geometry information as guidance for inpainting. Liu *et al.* [?] integrate perceptual subnetwork to capture semantic-level facial features, thus improving synthesized content details. While these methods [?], [?] focus on the correctness of the structural information, they neglect the quality of the texture on key areas in the image (*e.g.*, key facial components). Zhou *et al.* [?] propose to learn the correlations between facial textures at multiple scales and take the location of the facial components as prior knowledge during the face inpainting process. Although [?] can produce high-fidelity face images with fine-grained facial components, it still suffers from severe performance degradation when inputs are in low resolutions.

III. PROPOSED METHOD: PRO-UIGAN

In this section, we propose a Progressive Upsampling and Inpainting Generative Adversarial Network (Pro-UIGAN) for joint face inpainting and SR. Our Pro-UIGAN comprises a Pro-UI-net and two discriminators, *i.e.*, Local-D and Global-D. The Pro-UI-net estimates facial geometry priors, *i.e.*, facial landmark heatmaps, and uses them as the semantic guidance to obtain non-occluded HR faces progressively. Meanwhile, the Local-D and Global-D enforce the hallucinated faces to be more photo-realistic.

A. Multi-stage Progressive Hallucination Strategy

Inspired by Bengio *et al.* [?], we define a reasonable multi-stage progressive hallucination strategy. The first stage produces a coarse hallucinated face from an occluded LR input, which acts as a preliminary result for its following stage to refine. Then, the following stage achieves refinement of the face image hallucinated at the previous stage and generates a finer hallucinated one, which provides more delicate prior knowledge for the next stage. By repeating procedures mentioned previously, we can super-resolve and inpaint the occluded LR face in a coarse-to-fine manner. It is empirically demonstrated that our proposed progressive learning manner and the designed network can reduce blurriness and artifacts in the hallucinated face image significantly, as shown in Fig. 4(l).

B. Pro-UI-net

Based on our multi-stage progressive hallucination strategy, our Pro-UI-net stacks a series of Upsampling and Inpainting Blocks (UI-blocks) and reconstructs non-occluded HR face images progressively (see Fig. 2).

First, an occluded LR face and its facial landmark features estimated by [?] are sent into the first UI-block. Our UI-block comprises a Cross-Modal Transformer Module (CM-TM) and a Transformative Upsampling Net (TUN). The CM-TM employs the input face and its landmark features as queries

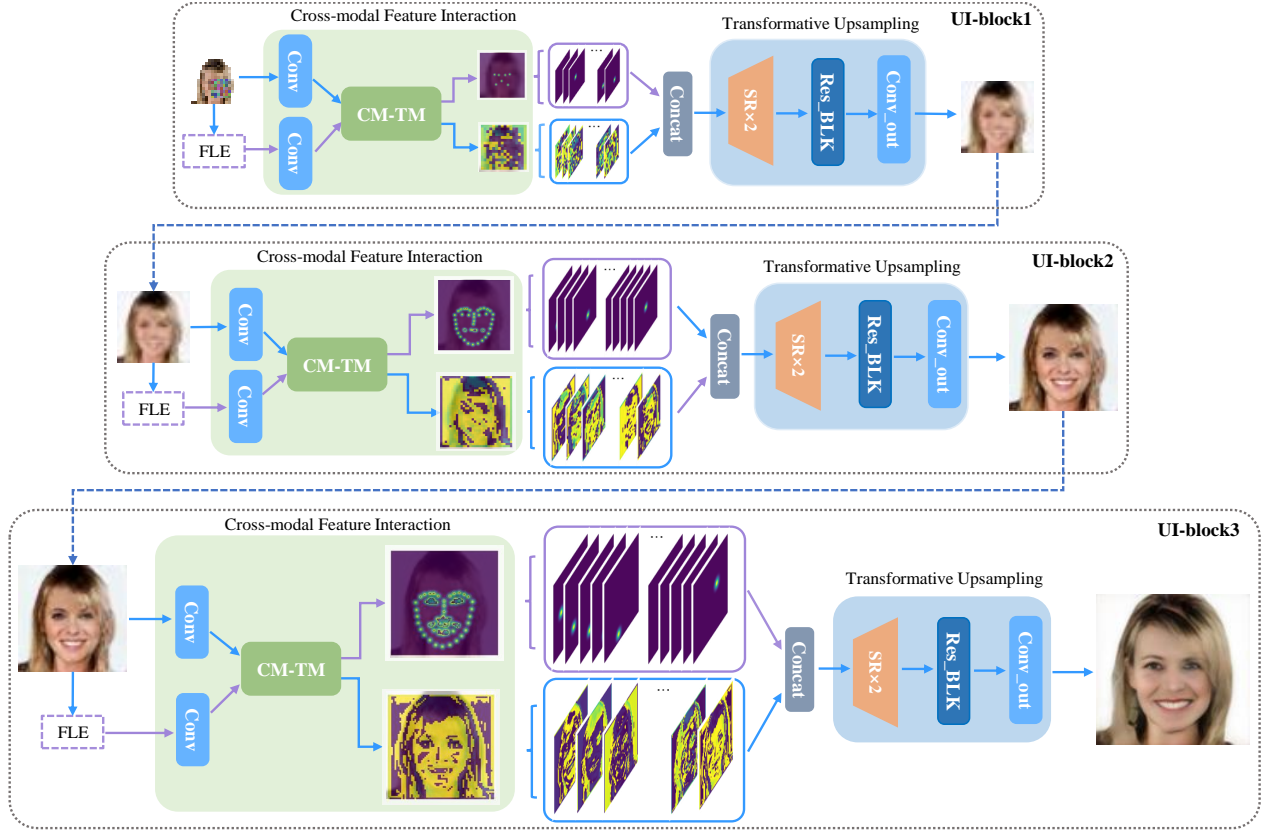


Fig. 2: The architecture of our Pro-UIInet. Here, FLE represents a facial landmark estimation model [?]. CM-TM represents the cross-modal transformer module.

and keys, and collaboratively learns facial geometry priors and facial appearance features. Then, the learned facial geometry priors and facial appearance features are concentrated and sent into the TUN for feature alignment, aggregation, and $2\times$ upscaling. Our TUN employs the residual block [?] to enhance high-frequency facial details while improving the network capacity. As a result, the first UI-block generates a coarse completed and upsampled face (see Fig. 4(c)). Subsequently, the latter UI-blocks further inpaint and upsample the coarse hallucinated face, generating finer hallucinated ones (see Figs. 4(d) and (l)). Specifically, as the stage number increases, the latest input image generated by the UI-block in the past stage, becomes more accurate in structures and provides more detailed prior knowledge, both of which benefit to learning processes in the current and following stages.

C. Cross-modal Transformer Module (CM-TM)

We argue that facial geometry priors (*i.e.*, facial landmark heatmaps) and facial appearance features are different but complementary. Thus, we design the CM-TM to learn facial geometry priors and facial appearance features in a mutual promotion manner.

As shown in Fig. 3, the facial landmark features F_L and the input facial features F_C are formulated as queries (Q) and keys (K) to calculate their cross-attention matrix. Then, the cross-attention matrix is adopted to augment the attended features from one stream to another. Such a design encourages joint

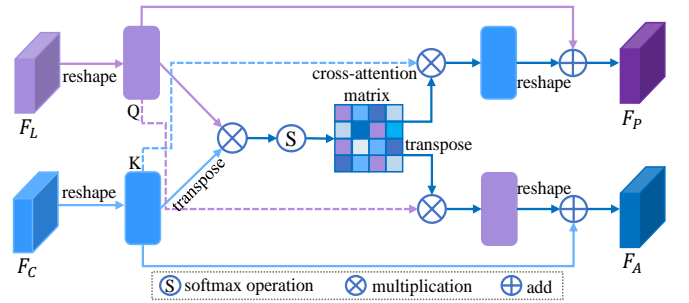


Fig. 3: The diagram of CM-TM. F_L , F_C , F_P and F_A represent facial landmark features, input facial features, facial geometry priors and facial appearance features, respectively.

feature learning across the input facial and landmark features, and their deep feature correspondences will be discovered by attention. As a result, we can learn the facial geometry priors (F_P) and facial appearance features (F_A).

To illustrate the effect of our CM-TM, we conduct some comparisons. Fig. 4(e) shows that the Pro-UIGAN variant without CM-TM produces inferior results. Therefore, our CM-TM provides effective facial geometry priors as clues for feature alignment and enhancement, and thus promotes more accurate face hallucination results (see Fig. 4(l)).

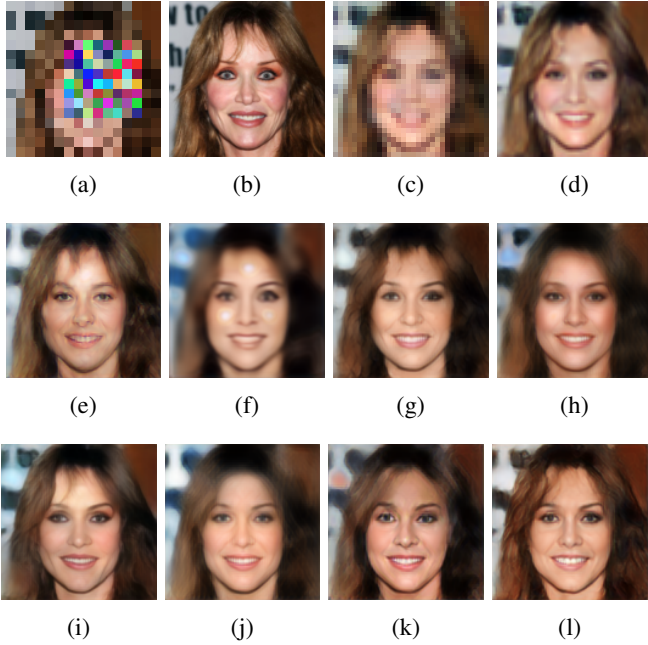


Fig. 4: Impacts of different components and losses on model performance. (a) Occluded LR images (16×16 pixels). (b) Ground-truth HR images (128×128 pixels). (c) Results of UI-block1. (d) Results of UI-block2. (e) Results of Pro-UIGAN without adopting CM-TMs. Note that the facial geometry is ambiguous. (f) Results of Pro-UIGAN trained by L_{mse} and L_h . (g) Results of Pro-UIGAN trained by L_{mse} , L_{id} and L_h . (h) Results of Pro-UIGAN without using the estimated facial geometry priors. Here, we just employ the facial appearance features as the input of TUNs. (i) Results of Pro-UIGAN using ground-truth facial geometry priors. (j) Results of Pro-UInet (Pro-UIGAN trained without employing L_{adv}^l and L_{adv}^g). (k) Results of Pro-UInet and Local-D. (l) Results of Pro-UIGAN.

D. Local-Global Discriminators

Our Pro-UInet upsamples occluded LR faces through a coarse-to-fine fashion and generates non-occluded HR face images. We employ two discriminators, *i.e.*, Global-D and Local-D, to force the generated HR faces to lie on the same manifold as real HR faces do. The Local-D encourages the newly generated missing parts to be semantically valid, while the Global-D focuses on the whole faces for more photo-realistic global views.

To dissect the impacts of Global-D and Local-D, we provide the results of different Pro-UIGAN variants (see Figs. 4(j), (k), and (l)). As shown in Fig. 4(k), the Pro-UInet with Local-D generates visually pleasing details of missing components. However, the global structure of the face is still blurry. This is because the Local-D can hardly generate a direct impact outside the missing regions during the back propagation. In contrast, as shown in Fig. 4(l), our Pro-UIGAN captures global profiles of faces and local facial characteristics.

E. Objective Functions

We incorporate six independent losses for training our Pro-UIGAN, including an intensity similarity loss (L_{mse}), an

identity similarity loss (L_{id}), a mirror symmetry loss (L_{sys}), a geometry similarity loss (L_h), a style loss (L_{style}) and a local-global discriminative loss (L_{adv}^l and L_{adv}^g).

1) *Intensity similarity loss*: We constrain the hallucinated face to be close to the ground-truth in terms of image intensities. Therefore, we employ an intensity similarity loss L_{mse} , expressed as:

$$L_{mse} = \mathbb{E}_{(\hat{h}_i, h_i) \sim p(\hat{h}, h)} \|\hat{h}_i - h_i\|_F^2, \quad (1)$$

where $p(\hat{h}, h)$ represents the joint distribution of the hallucinated face \hat{h}_i and the corresponding ground-truth h_i .

2) *Identity similarity loss*: As the intensity similarity loss L_{mse} leads to over-smoothed results [?] (see Fig. 4(f)), we introduce an identity similarity loss [?] to improve our hallucinated faces. The identity similarity loss L_{id} measures the Euclidean distance between the high-level features of a hallucinated face and its ground-truth, written as:

$$L_{id} = \mathbb{E}_{(\hat{h}_i, h_i) \sim p(\hat{h}, h)} \|\Phi(\hat{h}_i) - \Phi(h_i)\|_F^2, \quad (2)$$

where $\Phi(\cdot)$ represents the extracted feature maps of a layer in VGG-19 [?]. We use the layer ReLU32, which gives good empirical results in our experiments. As seen in Fig. 4(g), exploiting L_{id} results in better hallucinated results with more photo-realistic facial details.

3) *Mirror symmetry loss*: In order to guarantee the content integrity of hallucinated faces, we use a mirror symmetry loss [?]. The mirror symmetry loss L_{sys} for an upsampled face \hat{h}_i is defined as:

$$L_{sym} = \mathbb{E}_{(\hat{h}_i) \sim p(\hat{h})} \|\vec{\hat{h}}_i - \hat{h}_i\|_F^2, \quad (3)$$

where $\vec{\hat{h}}_i$ is the horizontally flipped copy of \hat{h}_i .

4) *Geometry similarity loss*: Aiming at facilitating face alignment as well as constraining the topological structure consistency between the generated HR image and the ground-truth one, a geometry similarity loss L_h [?] is employed in training our CM-TMs, expressed as:

$$L_h = \mathbb{E}_{(l_i, h_i) \sim p(l, h)} \frac{1}{L} \sum_{l=1}^L \|H^k(f_i) - H^k(h_i)\|_2^2, \quad (4)$$

where $H^k(f_i)$ represents the estimated k -th facial landmark heatmap by our CM-TM. $H^k(h_i)$ denotes the corresponding facial landmark heatmap generated by FAN [?] on the ground-truth image h_i .

5) *Style loss*: Inspired by [?], we introduce a style loss L_{style} to enforce the style of the completed area as similar as possible to the ground-truth image. The style loss L_{style} is defined as:

$$L_{style} = \sum_{n=0}^{N-1} \left\| K_n \left(\phi_n(\hat{h}_i)^T \phi_n(\hat{h}_i) - \phi_n(h_i)^T \phi_n(h_i) \right) \right\|_1, \quad (5)$$

where $\phi_n(\cdot)$ represents the extracted feature maps of the n -th layer in VGG-16 [?], and we use the pool1, pool2 and pool3 layers. $K_n = 1 / (C_n \cdot H_n \cdot W_n)$ is a normalization factor for the n -th VGG-16 layer. C_n , H_n , and W_n are the channel number, height, and width of the feature maps, respectively.

6) *Local-Global discriminative loss*: In order to generate visually appealing results, we incorporate class-specific discriminative information into our Pro-UINet by employing local-global discriminators, *i.e.*, Local-D and Global-D. Our goal is to fool the local-global discriminators and make them fail to classify hallucinated images and real ones.

The objective function L_D^l for the Local-D is defined as follows:

$$L_D^l = -\mathbb{E}_{(\hat{m}_i, m_i) \sim p(\hat{m}, m)} \left[\log D_u^l(m_i) + \log(1 - D_u^l(\hat{m}_i)) \right], \quad (6)$$

where $p(\hat{m}, m)$ represents the joint distribution of reconstructed occluded areas \hat{m}_i and corresponding ground-truths m_i . D^l and u represent the Local-D and its parameters. To make the Local-D distinguish hallucinated occluded areas from real ones, we minimize the loss L_D^l and update its parameters u .

The objective function L_D^g for the Global-D is defined as follows:

$$L_D^g = -\mathbb{E}_{(\hat{h}_i, h_i) \sim p(\hat{h}, h)} \left[\log D_v^g(h_i) + \log(1 - D_v^g(\hat{h}_i)) \right], \quad (7)$$

where D^g and v represent the Global-D and its parameters. To enable the Global-D to distinguish hallucinated faces from real ones, we minimize the loss L_D^g and update its parameters v .

For the generator in our Pro-UINet, it aims to fool the local-global discriminators by producing realistic non-occluded HR faces.

Thus, the local discriminative loss L_{adv}^l is written as:

$$L_{adv}^l = -\mathbb{E}_{\hat{m}_i \sim p(\hat{m})} \log(D_u^l(\hat{m}_i)). \quad (8)$$

Meanwhile, the global discriminative loss L_{adv}^g is represented as:

$$L_{adv}^g = -\mathbb{E}_{\hat{h}_i \sim p(\hat{h})} \log(D_v^g(\hat{h}_i)). \quad (9)$$

In the network learning process, we minimize L_{adv}^l and L_{adv}^g .

F. Training Details

Although UI-block1, UI-block2, and UI-block3 tackle the same hallucination subtask, their different inputs with diverse details attach their learning process with varying levels of difficulty. Therefore, we adopt different loss terms for training different UI-blocks.

The objective function for the UI-block1, L_{net1} , is expressed as:

$$L_{net1} = L_{sys}^a + L_{mse}^a + \alpha L_{id}^a + \beta L_h^a + \gamma^a L_{style}^a. \quad (10)$$

The objective function for the UI-block2, L_{net2} , is expressed as:

$$L_{net2} = L_{mse}^b + \alpha L_{id}^b + \beta L_h^b + \gamma^b L_{style}^b. \quad (11)$$

The objective function for the UI-block3, L_{net3} , is expressed as:

$$L_{net3} = L_{mse}^c + \alpha L_{id}^c + \beta L_h^c + \gamma^c L_{style}^c + \psi(L_{adv}^l + L_{adv}^g). \quad (12)$$

Consequently, the total objective function of our Pro-UINet, L_G is written as:

$$L_G = L_{net1} + L_{net2} + L_{net3}. \quad (13)$$

Since we aim to force hallucinated HR faces to be similar to real ones, we set lower weights on L_{id} , L_h , L_{adv}^l and L_{adv}^g . Thus, α, β and ψ in Eqs. (10)–(12) are set to 0.01. Meanwhile, γ^a, γ^b and γ^c are set to 10, 10 and 1, respectively.

The training procedure of our Pro-UIGAN model includes three steps: (i) Pre-training the UI-block1 with loss L_{net1} (Eq. (10)) so as to initialize model parameter. (ii) Pre-training the UI-block2 with loss L_{net2} (Eq. (11)). In this stage, the UI-block1 has been initialized. (iii) Training the whole Pro-UIGAN model: Pro-UINet is trained by L_G (Eq. (13)), and L_D^l (Eq. (6)) and L_D^g (Eq. (7)) are used to optimize Local-D and Global-D. In step (iii), since our UI-block1 and UI-block2 have been initialized, the learning rates for training UI-block3, UI-block2, and UI-block1 are set to 10^{-3} , 10^{-4} , and 10^{-4} , respectively.

IV. EXPERIMENTS

A. Experimental Setup

1) *Databases*: Our Pro-UIGAN is trained and tested on popular face databases, *i.e.*, the CelebA-HQ database [?], the Multi-PIE database [?], and the Helen database [?].

Multi-PIE [?] provides 750K+ images of 337 individuals under different conditions. We select 12,912 images of all the individuals spanning across various poses (0° , $\pm 15^\circ$, $\pm 30^\circ$, $\pm 45^\circ$, $\pm 60^\circ$, $\pm 75^\circ$, $\pm 90^\circ$) as well as expressions (“squint”, “disgust”, “neutral”, “smile”, “surprise”, and “scream”). Our training set contains 12,000 images belonging to the former 250 individuals, and the testing set includes 912 images belonging to the remaining 87 individuals.

CelebA-HQ [?] consists of 30,000 high-resolution face images under various poses, expressions and backgrounds. Each face image has a manually annotated, binary segmentation mask as well as 19 labeled facial attributes, *e.g.*, eyes, mouth, hat, neck, skin, etc. We employ the standard split for CelebA-HQ in our experiments, where 28,432 images for training and 1,568 for testing.

Helen [?] is composed of 2,330 in-the-wild face images with labeled facial components, *e.g.*, eyebrows, lips, nose, skin, hairs, etc. We use the former 2,280 images to construct the training set, and the remaining 50 images form the testing set. Specifically, we conduct data augmentation for the training set. We rotate the face images by $\pm 90^\circ$, $\pm 180^\circ$, $\pm 270^\circ$ and then flip them horizontally. As a result, we augment seven additional images for each original one.

2) *Implementation details*: First, faces in all the databases are detected, cropped, and resized to 128×128 pixels and thus form our ground-truths. Then, we use the masks with different sizes, ranging from 16×16 to 64×64 pixels, and covering at least one critical facial component to construct the occluded HR faces. Note that the position of the mask is randomly selected. Afterward, we generate the occluded LR faces (16×16 pixels) by transforming and downsampling the occluded HR ones. As a result, we construct occluded LR/non-occluded HR face pairs for each database. Our large-scale occluded LR/non-occluded HR face pair dataset and the code will be available on <https://github.com/SEU-yang>.

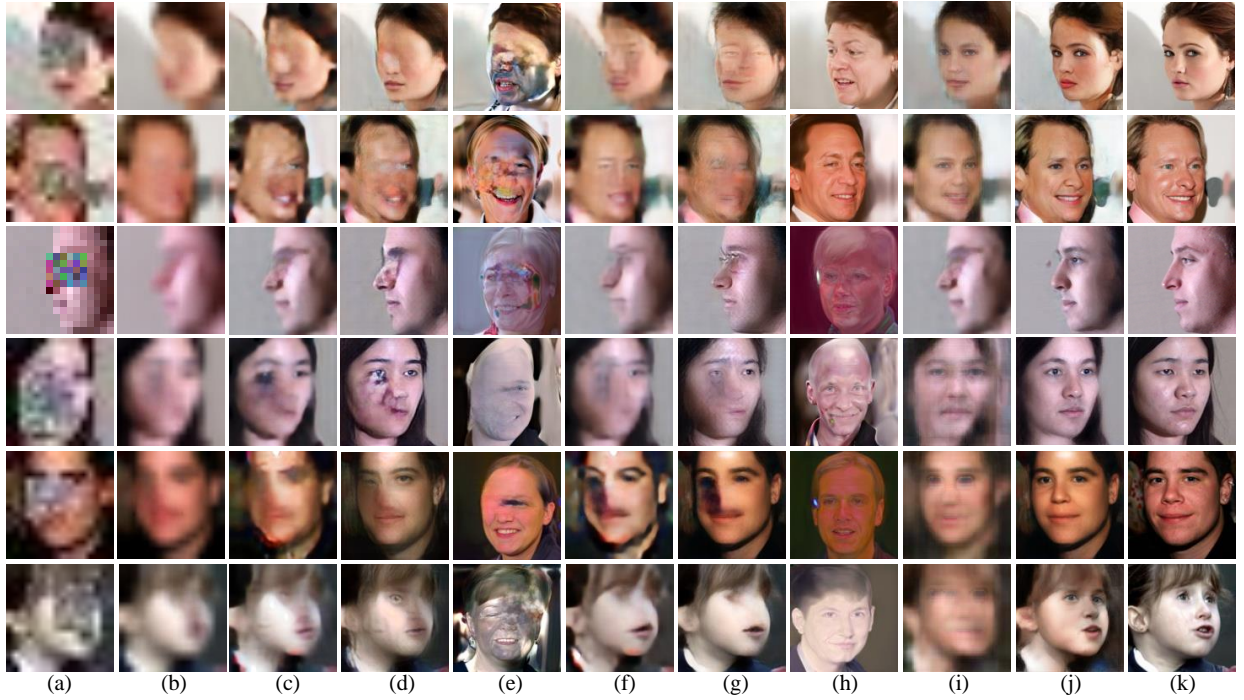


Fig. 5: Qualitative comparisons of competing methods on the **CelebA-HQ**, **Multi-PIE**, and **Helen** databases. Columns: (a) Occluded LR faces (16×16 pixels). (b) Bicubic + [?]. (c) [?] + [?]. (d) [?] + [?]. (e) [?] + [?]. (f) [?] + [?]. (g) [?] + [?]. (h) [?] + [?]. (i) [?]. (j) Ours. (k) Ground-truths. The first two lines: testing samples from **CelebA-HQ**. The middle two lines: testing samples from **Multi-PIE**. The last two lines: testing samples from **Helen**.

TABLE I: Quantitative comparisons of competing methods on the **CelebA-HQ**, **Multi-PIE**, and **Helen** databases.

SR Method	CelebA-HQ		Multi-PIE		Helen		CelebA-HQ		Multi-PIE		Helen	
	SR+PA [?]						PA [?]+SR					
	PSNR	SSIM	PSNR	SSIM	PSNR	SSIM	PSNR	SSIM	PSNR	SSIM	PSNR	SSIM
Bicubic	14.038	0.411	12.761	0.370	13.665	0.389	15.322	0.457	14.215	0.416	13.763	0.392
FSRnet [?]	15.011	0.451	13.538	0.403	14.086	0.423	16.445	0.482	15.386	0.459	14.342	0.420
FHC [?]	16.950	0.503	16.448	0.482	16.003	0.476	19.224	0.609	18.198	0.573	17.715	0.546
PULSE [?]	13.106	0.353	8.451	0.182	10.516	0.273	15.270	0.456	9.237	0.206	11.128	0.294
FCSR-GAN [?]	23.010	0.698	21.327	0.649	20.745	0.627	23.010	0.698	21.327	0.649	20.745	0.627
Pro-UIGAN	25.470	0.763	23.188	0.704	22.038	0.659	25.470	0.763	23.188	0.704	22.038	0.659

3) *Competing methods*: We conduct comparative experiments in the following three manners:

- SR+PA: face SR methods (FSRnet [?], FHC [?], or PULSE [?]) followed by face inpainting techniques (GFC [?]);
- PA+SR: face inpainting techniques (GFC [?]) followed by face SR methods (FSRnet [?], FHC [?], or PULSE [?]) (bicubic interpolation is used to resize images);
- Joint SR+PA: FCSR-GAN [?] and our Pro-UIGAN.

In the first manner (SR+PA), we upsample the occluded LR faces first and then inpaint the upscaled results. In the second manner (PA+SR), we first inpaint occluded LR faces by widely-used face inpainting techniques and then upsample the completed faces by SotA face SR methods. In the third manner (Joint SR+PA), both FCSR-GAN [?] and Pro-UIGAN handle face SR and face inpainting in a unified framework. Here, we retrain these compared methods on our training datasets for fair comparisons.

B. Qualitative Evaluation

Fig. 5 illustrates the qualitative results of the compared methods.

As visible in Fig. 5(b), different combinations of bicubic interpolation and face inpainting methods [?] fail to reconstruct authentic facial details. Because bicubic only interpolates new pixels from neighboring ones, it can not produce new contents and upsampled HR images lack details. Consequently, the face inpainting method fails to segment facial areas and generates erroneous results with notorious ambiguity, such as over-smoothed facial details and distorted contours.

As analyzed in Sec. I, directly utilizing SotA face SR and inpainting methods fails to solve this challenging problem. Therefore, the results of SR+PA and PA+SR methods suffer from corrupted facial regions and ghosting artifacts (see Figs. 5(c)-(h)).

Since FCSR-GAN super-resolves and inpaints occluded LR faces in an integrated framework, it avoids exaggerating errors

TABLE II: Ablation study of facial geometry priors.

	CelebA-HQ		Multi-PIE	
	PSNR	SSIM	PSNR	SSIM
P-FP	21.739	0.648	19.325	0.602
P+GT	26.340	0.791	24.007	0.733
Pro-UIGAN	25.470	0.763	23.188	0.704

TABLE III: Ablation study of different training losses.

	CelebA-HQ		Multi-PIE	
	PSNR	SSIM	PSNR	SSIM
L_G^-	19.136	0.605	18.473	0.579
L_G^+	20.872	0.628	19.281	0.610
L_G^\dagger	22.359	0.664	20.403	0.619
L_G^*	24.960	0.756	22.755	0.674
L_G	25.470	0.763	23.188	0.704

caused by model combination and generates relatively satisfying results. However, FCSR-GAN is a single-stage model, which does not possess a “looking back” ability to revise upsampled HR faces. Consequently, when the input LR faces are under large poses or complex expressions (see Fig. 5(a)), FCSR-GAN produces blurry HR faces, as seen in Fig. 5(i).

As shown in Fig. 5(j), our Pro-UIGAN generates visually appealing non-occluded HR faces from very LR and occluded inputs. Specifically, we show challenging examples with extreme poses and expressions (*e.g.*, the first, third, and sixth lines in Fig. 5(a)). It demonstrates that the hallucinated faces of our Pro-UIGAN are more authentic and vivid. Pro-UIGAN exploits a multi-stage progressive hallucination strategy and thus refines the hallucinated faces gradually, thus achieving superior hallucination performance.

C. Quantitative Evaluation

To evaluate the hallucination performance quantitatively, we provide the average Peak Single-to-Noise Ratio (PSNR) and Structural Similarity (SSIM) values of all methods on the testing sets in Tab. I.

Tab. I shows that our Pro-UIGAN obtains the best quantitative results in comparison to the SotA methods on all the databases. For example, on the CelebA-HQ testing set, Pro-UIGAN surpasses the other baselines by improving the PSNR by 8.7% dB. This is mainly because our model progressively refines hallucinated results via a coarse-to-fine manner. Furthermore, Tab. I also indicates that inpainting followed by super-resolution leads to slightly higher quantitative results than super-resolution followed by inpainting. This implies that super-resolving non-occluded LR facial patterns are easier than occluded ones.

D. Ablation Analysis

1) *Impacts of facial geometry priors:* In our work, we exploit facial geometry priors, *i.e.*, facial landmark heatmaps, for joint face SR and inpainting. We give a full discussion about how many improvements the facial geometry priors bring.

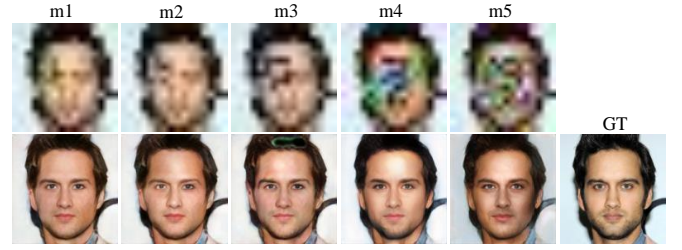


Fig. 6: Qualitative evaluation on different mask sizes.

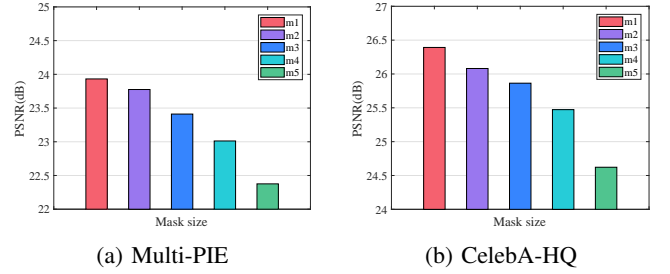


Fig. 7: Quantitative evaluation on different mask sizes.

We formulate two baseline models as below (we denote Pro-UIGAN as P, estimated facial priors as FP, and ground-truth facial priors as GT):

- P-FP: we discard the estimated facial priors of CM-TMs and employ the facial appearance features as the input of TUNs.
- P+GT: we use ground-truth facial landmark heatmaps instead of estimated facial priors, denoted by the “P+GT” model.

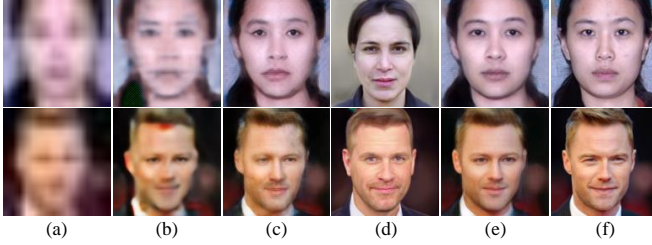
As illustrated in Fig. 4, the result of “P+GT” model (see Fig. 4(i)) shows more accurate facial geometry than the results of “P-FP” model (see Fig. 4(h)) and our Pro-UIGAN (see Fig. 4(l)). This implies the importance of facial geometry priors in the hallucination process: accurate facial prior knowledge assists in reducing the ambiguous mapping caused by occlusions and thus facilitates the upsampling procedures. As shown in Tab. II, the P+GT model (with the ground-truth facial geometry priors) outperforms the Pro-UIGAN model (with the estimated facial geometry prior) and P-FP model (without prior information) with the PSNR improvement of 0.819 dB and 4.682 dB on CelebA-HQ, respectively. Consequently, facial geometry priors significantly promote the model performance and thus achieve high-quality hallucinated results.

2) *Impact of different losses:* We provide the results of our Pro-UIGAN trained by using different losses on Multi-PIE and CelebA-HQ (see Tab. III and Fig. 4). We denote the compared Pro-UIGAN variants as follows: (i) L_G^- : L_{mse} and L_h ; (ii) L_G^+ : L_{mse} , L_{id} , and L_h ; (iii) L_G^\dagger : L_{mse} , L_{id} , L_h , and L_{sys} ; (iv) L_G^* : L_{mse} , L_{id} , L_h , L_{sys} , L_{style} , and L_{adv}^l ; (v) L_G : L_{mse} , L_{id} , L_h , L_{sys} , L_{style} , L_{adv}^l , and L_{adv}^g . Note that L_h is a prerequisite constraint in training our CM-TMs.

Fig. 4(f) shows that only exploiting the intensity similarity loss L_{mse} results in overly smooth results. Therefore, we introduce an identity similarity loss L_{id} to improve the visual quality (see Fig. 4(f)). The same results are confirmed by

TABLE IV: Efficiency comparisons on the CelebA-HQ testing set.

Method		Model Size (KB)	Running Time (ms)	PSNR (dB)
PA+SR SR+PA	FSRnet [?]	69,200	286.08	16.445/15.011
	FHC [?]	71,700	289.12	19.224/16.950
	PULSE [?]	118,500	5128.36	15.270/13.106
Joint SR+PA	FCSR-GAN [?]	112,200	145.69	23.010
	Pro-UIGAN	42,000	34.21	25.470

Fig. 8: Comparisons with SotA face SR methods. Columns: (a) Non-occluded LR inputs (16×16 pixels). (b) FSRnet [?]. (c) FHC [?]. (d) PULSE [?]. (e) Ours. (f) Ground-truth HR images (128×128 pixels).

the quantitative results in Tab. III (*i.e.*, L_G^- and L_G^\dagger). To guarantee the content integrity of completed faces, the mirror symmetry loss L_{sys} is employed for training our network. L_{sys} reduces the reconstruction errors during the training procedure and improves the model performance (see L_G^\dagger in Tab. III). Furthermore, as indicated in Tab. III (L_G^\dagger) and Fig. 4(k), the Local-D improves the model performance. However, the face in Fig. 4(k) still suffers from global structural inconsistency. Finally, after incorporating Global-D, Pro-UIGAN achieves the most satisfying faces (see Fig. 4(l)) and the best quantitative results (L_G in Tab. III).

E. Impacts of Different Mask Sizes

We evaluate the impact of different mask sizes on our model. The compared masks are as follows: (a) m1: 16×16 , (b) m2: 24×24 , (c) m3: 32×32 , (d) m4: 48×48 , (e) m5: 64×64 .

Figs. 6 and 7 show the qualitative and quantitative results of LR faces with different masks. The performance of our Pro-UIGAN gradually drops when the mask size increases. This is expected as larger mask sizes indicate more uncertain pixel values. But generally, our Pro-UIGAN performs well for all mask sizes, even when the occluded region is with a large size (*i.e.*, m5). Our facial geometry priors ensure the integrity of the facial structure and the consistency of facial attributes for the generated results, thus ensuring satisfying inpainting performance.

F. Efficiency Analysis

We provide efficiency comparisons for our Pro-UIGAN and the competing baselines in Tab. IV. Compared with the SotA methods, our Pro-UIGAN requires the shortest running time

(34.21 ms) because Pro-UIGAN performs face SR and inpainting seamlessly. Moreover, despite our multi-stage framework, Pro-UIGAN is more lightweight than the compared models. Note that we achieve the best quantitative results as indicated by the PSNR in Tab. IV. As a result, our Pro-UIGAN model is computationally efficient and functionally prominent.

G. Facial Attributes Manipulation

After hallucinating the occluded LR faces, users may not be satisfied with the generated facial attributes and want to manipulate them. We demonstrate that our model allows the users to conduct interactive facial attribute editing on the hallucinated face. As shown in Fig. 9, we can change the facial geometry priors to modify one attribute (*i.e.*, mouth, nose, or eyes) while other attributes are maintained similar to the ground-truth.

H. Performance on Non-occluded LR Faces

As illustrated in Fig. 1(d), the face inpainting method [?] fails to inpaint LR faces and produces inferior results. Then, the errors would be exaggerated in the following face SR process (see Fig. 1(f)). In contrast, we jointly inpaint and super-resolve occluded LR faces rather than tackling these two tasks separately. Hence, we alleviate the side-effects of direct model combination.

For fair comparisons, we conduct experiments to evaluate Pro-UIGAN and SotA face SR methods on non-occluded LR faces. In this case, face inpainting methods are not indispensable and thereby not employed. According to the results in Fig. 8, Pro-UIGAN still outperforms the SotA methods and achieves more visually appealing and identity-preserving results. This demonstrates the effectiveness of our progressive learning strategy and the identity-preserving ability of our model.

I. Performance on Faces with Real Occlusions

We demonstrate our method can effectively hallucinate the faces where real occlusions occur. We select a few CelebA-HQ testing faces partly occluded by objects such as glasses or microphones. Since such regions in the images are occluded or not is subjective, we give users this option to appoint the occluded regions through appending masks. Then, we obtain the occluded LR faces (16×16 pixels) by transforming and downsampling the processed images. As shown in Fig. 10, our model not only hallucinates the visually appealing HR faces but also removes the real occlusions. Furthermore, we present the cosine distances between LR faces, hallucinated HR faces, and their ground-truths (see Fig. 10). Here, we employ a SotA pre-trained face recognition model (ArcFaceNet [?]) to extract the deep features for calculation. As a result, our Pro-UIGAN reconstructs face images with high-fidelity identity information, in comparison to the SotA [?].

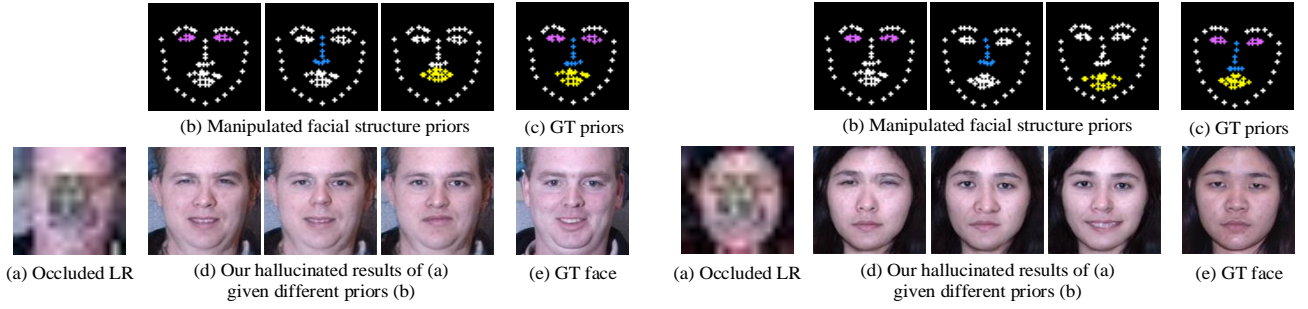


Fig. 9: Facial attribute editing results.

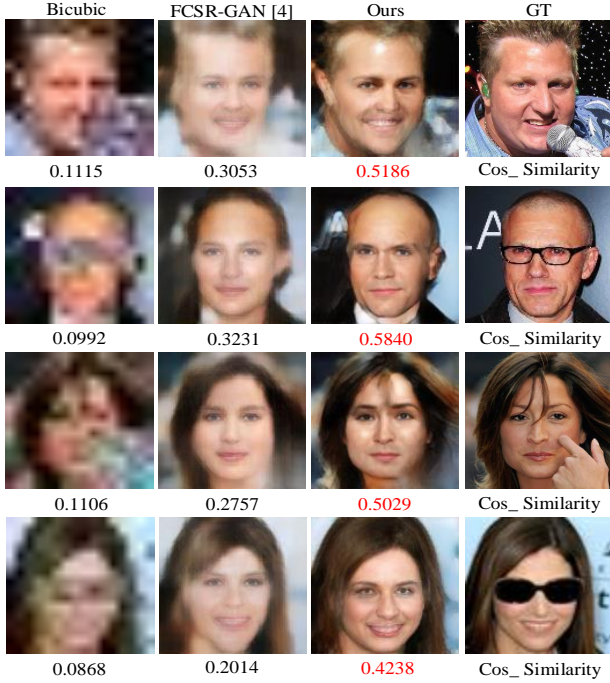


Fig. 10: Face hallucination results of real occlusions.

V. FACE HALLUCINATION EVALUATION VIA DOWNSTREAM TASKS

A. Comparisons with SotA on Face Alignment

We demonstrate that our Pro-UIGAN boosts the performance of low-quality face alignment. We adopt the “alignment via hallucination” framework to conduct experiments on the **CelebA-HQ**, **Multi-PIE**, and **Helen** databases. Specifically, occluded LR faces are hallucinated by compared methods first and then used for alignment.

Fig. 11 shows the hallucinated images of compared methods and the facial landmarks estimated by FAN [?] on different hallucinated faces. Moreover, Tab. IV provides the NRMSE performance, which is a commonly used metric in face alignment. The results indicate that: (1) It is a challenge for SotA face alignment models to predict landmarks directly from occluded LR face images. The predicted landmarks of the bicubic face suffer from significant errors around the eyes, mouth, or noses. However, our Pro-UIGAN can alleviate the alignment difficulty and thus results in lower NRMSE values than bicubic faces (see Tab. V). (2) In comparison with FCSR-GAN [?],

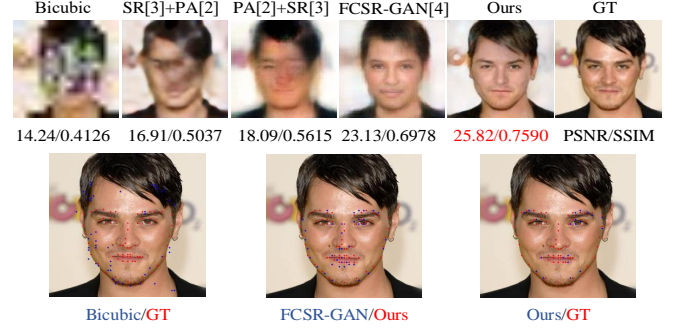


Fig. 11: Qualitative comparisons of face alignment.

our hallucinated face provides visually superior estimation on facial components and shapes, achieving the lowest NRMSE values on all datasets. These results demonstrate that Pro-UIGAN reconstructs facial geometry more accurately and is practical for low-quality face alignment tasks.

B. Comparisons with SotA on Face Parsing

We manifest that our Pro-UIGAN also benefits low-quality face parsing tasks. Similarly, we adopt an off-the-shelf face parsing model [?] to conduct face parsing experiments for recovered images of compared methods.

As shown in Fig. 12, the parsing maps of our hallucinated face images separate complete and accurate facial components, while others provide wrong shapes or lose components (*i.e.*, eyes, nose, or mouth). Meanwhile, we report the Intersection-over-Union (IoU) results on the testing sets with comparisons to the SotA (see Tab. V). As shown in Tab. V, our Pro-UIGAN yields the highest parsing accuracy and surpasses the competing methods by a large margin (over 5%) in terms of IoU on all databases. The comparison implies that Pro-UIGAN is a better method to reconstruct semantic-level facial features, thus positively affecting low-quality face parsing.

C. Comparisons with SotA on Face Recognition

The cosine distances in Fig. 12 partly reveal the identity-preserving ability of our model. In this section, we conduct face recognition experiments to discuss how much the face identity information can be preserved. This task simulates an open problem: occluded and low-resolution face recognition.

TABLE V: Quantitative comparisons on face alignment (NRMSE) and face parsing (IoU).

SR Method	CelebA-HQ		Multi-PIE		Helen		CelebA-HQ		Multi-PIE		Helen	
	SR+PA [?]						PA [?]+SR					
	NRMSE	IoU	NRMSE	IoU	NRMSE	IoU	NRMSE	IoU	NRMSE	IoU	NRMSE	IoU
Bicubic	30.67	0.0071	33.21	0.0074	35.64	0.0076	27.31	0.0076	29.56	0.0083	32.33	0.0082
FSRnet [?]	22.03	0.3484	24.68	0.3233	26.11	0.3192	20.13	0.3609	22.31	0.3404	23.74	0.3326
FHC [?]	18.35	0.4153	20.11	0.4049	20.87	0.3990	16.57	0.4318	17.32	0.4229	18.26	0.4166
PULSE [?]	40.07	0.1740	52.08	0.0646	44.35	0.1069	38.79	0.1834	49.22	0.0718	40.13	0.1261
FCSR-GAN [?]	9.74	0.5445	10.57	0.5231	11.69	0.4870	9.74	0.5445	10.57	0.5231	11.69	0.4870
Pro-UIGAN	7.31	0.6008	8.34	0.5822	9.96	0.5633	7.31	0.6008	8.34	0.5822	9.96	0.5633
Ground-truth HR	4.27	0.6501	2.58	None	3.84	0.6056	4.27	0.6501	2.58	None	3.84	0.6056

For Multi-PIE, parsing maps from ground-truth HR images are used as ground-truths.

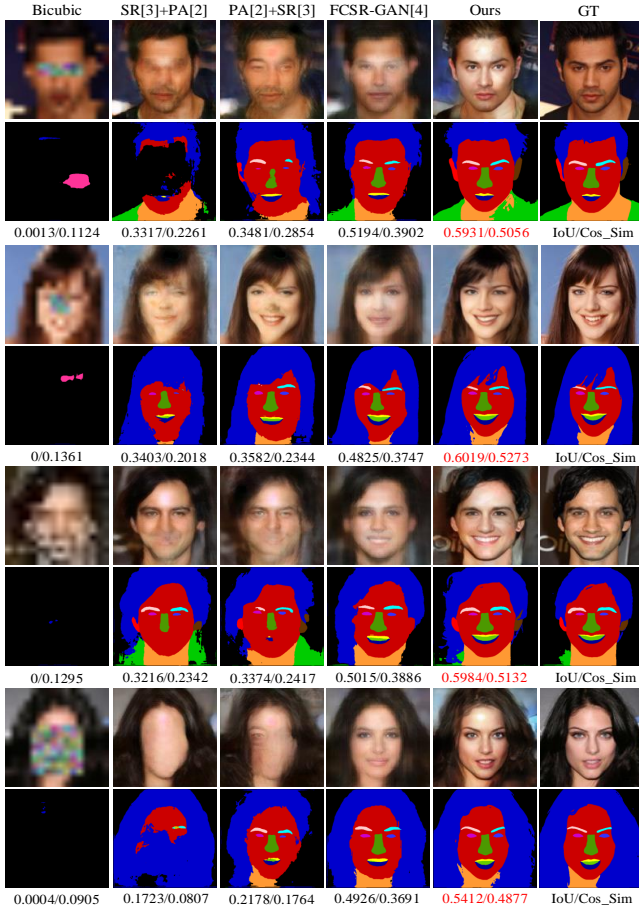


Fig. 12: Qualitative comparisons of face parsing.

1) *Experimental settings*: We use the “recognition via hallucination” scheme to conduct experiments on **Multi-PIE** [?]. First, we split the Multi-PIE face images according to the identity ID and construct subject disjoint training and testing sets. Then, we train the competing methods on the training set and conduct face recognition experiments on the testing set. Here, we choose the frontal HR face images of testing individuals to form our testing set. We apply the four masking types in Fig. 12 for each HR face. These masking types simulate the most common occlusions in the real world. For example, masking mouths simulates wearing masks, and masking eyes

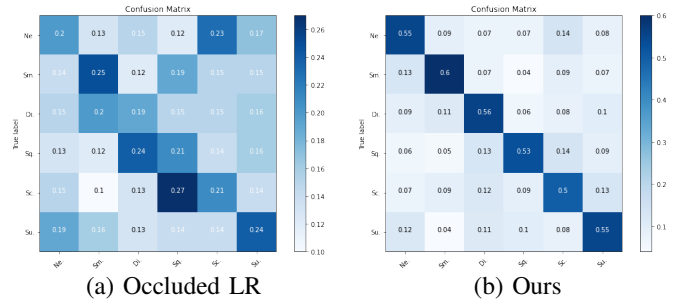


Fig. 13: Face recognition results for compared methods on Multi-PIE.

simulates wearing glasses. Subsequently, we generate occluded LR faces by downsampling and transforming the masked HR ones. Finally, we use a SotA pre-trained face recognition model [?] to conduct face recognition experiments on occluded LR faces and hallucinated non-occluded HR faces generated by compared methods.

2) *Evaluation*: As shown Fig. 13, the face recognition rate of our hallucinated faces outperforms those of the occluded LR faces and the compared methods’ results. This demonstrates that our Pro-UIGAN possesses significant identity preservation ability and benefits low-quality face recognition tasks.

D. Comparisons with SotA on Face Expression Classification

We demonstrate that Pro-UIGAN can preserve facial expressions and boost the performance of low-quality face expression classification.

1) *Experimental settings*: We conduct a standard 10-fold subject-independent cross-validation [?], [?] on **Multi-PIE** [?]. First, we split the synthesized occluded LR/non-occluded HR Multi-PIE face pairs according to the identity ID and form 10 subject-independent subsets. Then, we conduct ten-fold validation experiments. In each experiment, we choose 9 subsets to construct the training set and the remaining one to form the testing set. The compared face hallucination models are first trained on the same training set and then used to upsample and inpaint the testing faces. We introduce a SotA expression classification model [?] to classify the facial expression of hallucinated faces. Finally, for each compared method, we calculate the average of the expression classification results

TABLE VI: Face expression classification results for compared methods on Multi-PIE

SR method	Accuracy	
	PA+SR	SR+PA
Bicubic	22.34%	20.59%
FSRnet [?]	24.07%	22.52%
PULSE [?]	27.40%	24.16%
FHC [?]	30.66%	28.31%
FCSR-GAN [?]	45.93%	
Occluded LR	22.14%	
Non-occluded HR	94.62%	
Pro-UIGAN	55.57%	

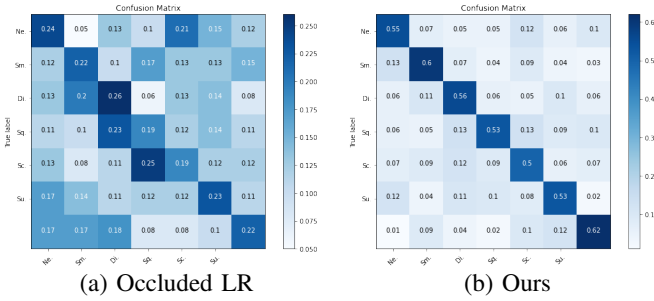


Fig. 14: The confusion matrices of LR faces and our hallucinated ones. Darker colors indicate higher accuracy.

of the 10 subsets. Here, we set the classification results of the occluded LR faces and the non-occluded HR ones as the lower and upper bounds for this task (see Tab. VI).

2) *Evaluation*: As shown in Tab. VI, the non-occluded HR faces hallucinated by our Pro-UIGAN achieve superior expression classification accuracy in comparison to the SotA. Meanwhile, we provide the confusion matrix for occluded LR faces and our hallucinated ones (see Fig. 14). It can be observed that the faces hallucinated by Pro-UIGAN outperform occluded-LR ones on all the expressions. These results indicate that Pro-UIGAN recovers authentic facial expressions and benefits low-quality face expression classification tasks.

VI. CONCLUSION

This paper presents a Pro-UIGAN framework to jointly super-resolve and inpaint occluded LR face images seamlessly. Moreover, our developed multi-stage progressive learning strategy allows us to achieve coarse-to-fine feature refinement under the guidance of facial geometry priors. Meanwhile, we provide a solution to estimating facial landmarks from occluded thumbnails, thus significantly improving our hallucination performance. Experimental results on multiple widely-used benchmarks confirm the efficacy of Pro-UIGAN in generating identity-preserving face images and substantially benefiting downstream tasks.